

Development of Biodegradable Osteopromotive Citrate-Based Bone Putty

Xinyu Tan, Ethan Gerhard, Yuqi Wang, Richard T. Tran, Hui Xu, Su Yan, Elias B. Rizk, April D. Armstrong, Yuxiao Zhou, Jing Du, Xiaochun Bai, and Jian Yang*

The burden of bone fractures demands development of effective biomaterial solutions, while additional acute events such as noncompressible bleeding further motivate the search for multi-functional implants to avoid complications including osseous hemorrhage, infection, and nonunion. Bone wax has been widely used in orthopedic bleeding control due to its simplicity of use and conformation to irregular defects; however, its nondegradability results in impaired bone healing, risk of infection, and significant inflammatory responses. Herein, a class of intrinsically fluorescent, osteopromotive citrate-based polymer/hydroxyapatite (HA) composites (BPLP-Ser/HA) as a highly malleable press-fit putty is designed. BPLP-Ser/HA putty displays mechanics replicating early non-mineralized bone (initial moduli from ≈ 2 –500 kPa), hydration induced mechanical strengthening in physiological conditions, tunable degradation rates (over 2 months), low swelling ratios (<10%), clotting and hemostatic sealing potential (resistant to blood pressure for >24 h) and significant adhesion to bone (≈ 350 –550 kPa). Simultaneously, citrate's bioactive properties result in antimicrobial ($\approx 100\%$ and 55% inhibition of *S. aureus* and *E. coli*) and osteopromotive effects. Finally, BPLP-Ser/HA putty demonstrates *in vivo* regeneration in a critical-sized rat calvaria model equivalent to gold standard autograft. BPLP-Ser/HA putty represents a simple, off-the-shelf solution to the combined challenges of acute wound management and subsequent bone regeneration.

(GBD) revealed that there were 178 million new fractures and 455 million prevalent cases of acute or long-term symptoms of a fracture in 2019, an increase of 33.4% and 70.1% since 1990, respectively. Traumatic bone fractures and surgical bone incisions in orthopedic surgeries often result in difficult-to-control osseous hemorrhage.^[1,2] Bone wax, a waxy and hydrophobic material mainly consisting of beeswax and softening agents such as Vaseline or a mixture of paraffin wax and isopropyl palmitate, can be easily applied to the bone fracture for bleeding control in orthopedic surgeries and many other procedures such as thoracic and neurological surgeries due to its ease of operation, satisfactory adhesion to bone, malleability, and cost-effectiveness.^[3,4] However, the obvious limitations and complications of bone wax counteracting its benefits for hemostasis and orthopedic applications include: 1) markedly impaired bone healing; 2) significant risk of infection; 3) inconsistent hemostatic efficacy; and 4) significant foreign body reactions.^[5–7] Therefore, current bone wax products should be restricted

in surgical sites where bone fusion is desirable and can never be used in contaminated wounds. Unfortunately, despite these known limitations, beeswax-based bone wax products

1. Introduction

Bone fracture is a major public health concern globally. A systematic analysis from the Global Burden of Disease Study

X. Tan, X. Bai
Department of Cell Biology
School of Basic Medical Sciences
Southern Medical University
Guangzhou, Guangdong Province 510515, China
X. Tan, E. Gerhard, Y. Wang, R. T. Tran, H. Xu, S. Yan, J. Yang
Department of Biomedical Engineering
Materials Research Institute
The Huck Institutes of the Life Sciences
The Pennsylvania State University
University Park, PA 16802, USA
E-mail: jxy30@psu.edu
X. Tan, X. Bai
Academy of Orthopedics
Provincial Key Laboratory of Bone and Joint Degenerative Diseases
The Third Affiliated Hospital of Southern Medical University
Guangzhou, Guangdong Province 510280, China

E. B. Rizk
Department of Neurosurgery
College of Medicine
The Pennsylvania State University
Hershey, PA 17033, USA
A. D. Armstrong
Department of Orthopaedics and Rehabilitation
College of Medicine
The Pennsylvania State University
Hershey, PA 17033, USA
Y. Zhou, J. Du
Department of Mechanical Engineering
The Pennsylvania State University
University Park, PA 16802, USA

 The ORCID identification number(s) for the author(s) of this article can be found under <https://doi.org/10.1002/smll.202203003>.

DOI: 10.1002/smll.202203003

remain the primary choice even more than 120 years after their inception.

There have been attempts in developing bioabsorbable bone wax to address the limitations and drawbacks of beeswax-based formulations. Claimed as an “absorbable bone wax”, a Pluronic (PPG-PEG-PPG copolymer)-based bone wax substitute, Ostene, was launched in 2006. Ostene can be manually softened and stuck to bleeding bone as a tamponade; however, it dissolves rapidly in 1–2 days. Although the rapid dissolution and absorption of Ostene may vacate the space for bone healing to occur, Ostene itself inherently lacks osteopromotive properties (osteoconductivity and/or osteoinductivity) to help bone healing, which greatly limits its use in bones with relatively large fractures and defects. Additionally, Pluronic itself is not considered “degradable”. Thus, its in vivo clearance remains a concern. In the past decade, bone wax has evolved into bone paste/putty to meet the demands for improved hemostasis and osteogenesis. Alginate, cellulose, or chitosan have been blended with ceramics such as tricalcium silicate cement, bioglass, or hydroxyapatite (HA) to develop bone putty.^[8–13] These bone-wax substitutes exhibit low cytotoxicity, biodegradability, and/or hemostatic functions and can also be used to deliver antibiotics, bone morphogenic proteins, and cytokines to overcome the potential risk of infection and improve bone healing.^[12,14,15] Bone glues, including commercial poly (methyl methacrylate) (PMMA), self-curing bone-wax substitute (consisting of tricalcium silicate, 58S bioglass, chitosan, carboxymethyl cellulose with KH_2PO_4 setting solution), and calcium phosphate cements (CPCs) were also used to enable hemostasis and bone healing. However, these formulations are limited by their slow degradation, necessary manual preparation steps, poor mechanical properties, insufficient fixation, moisture sensitivity, and/or inhibition of bone regeneration.^[16–18] Ideal bone wax or bone putty should be: 1) ready-to-use (no preparation steps); 2) easily press-fit but sufficiently strong (comparable to cancellous bone); 3) strongly adhesive to bone; 4) hemostatic; 5) osteopromotive; 6) antimicrobial; and 7) biodegradable and bioabsorbable. However, none of the existing bone waxes or bone putties can meet all the above requirements in a single formulation.

Citrate-based biomaterials have received significant attention in recent years. Citric acid not only participates in degradable bond formation in polymers,^[19] but also enhances hemocompatibility,^[20] balancing the hydrophilicity/hydrophobicity of polymers,^[19] confers antimicrobial properties,^[21] and provides additional binding sites for bioconjugation.^[22] Citrate-based biodegradable polymers developed include strong yet elastic crosslinked urethane-doped polyesters (CUPE) and clickable Poly (octamethylene-citrate) (POC)-based elastomers (POC-click) for vascular and bone tissue engineering,^[23–26] poly(alkylene maleate citrate) (PAMC) for injectable-based tissue engineering and endoscopic surgery,^[27–30] biodegradable photoluminescent polymers (BPLP) for tissue engineering and fluorescent imaging,^[31–34] and injectable citrate-based mussel-inspired bioadhesives (iCMBA) for sutureless wound closure.^[35,36] All citrate-based biodegradable polymers investigated including POC, PAMC, BPLP, and CUPE showed considerable antimicrobial properties against Gram-negative *E. coli* and Gram-positive *S. aureus*.^[37] Interestingly, the –COOH rich citrate-presenting elastomers were able to composite up to 65 wt% HA in

polymer/HA composites due to the chelation of citrate with calcium-containing particles, simulating the inorganic composition of natural bone, in contrast to traditional degradable polymers such as polylactide (PLA), which could only composite up to 25–30 wt% of HA to avoid brittleness of the composites.

One of these citrate polymers, poly(octamethylene citrate) (POC),^[38] has recently joined a handful of biodegradable synthetic polymers that have been developed into Food and Drug Administration (FDA)-approved/cleared medical devices. A series of POC-based bone screws and suture anchors such as Citrelock, Citrefix, and Citrespline for various orthopedic indications including knee, foot and ankle, shoulder, elbow, and wrist applications have recently received US FDA 510 K clearance and are currently being distributed for the sports injury market. The regulatory success of POC-based medical devices has spurred significant interest in further developing POC into various medical devices. We have also demonstrated by incorporating amino acids during the synthesis of POC, the resultant BPLPs exhibit tunable fluorescent properties that enable imaging and sensing applications.^[39,40] More interestingly, citrate has been identified as an osteopromotive factor to mediate the metabolism and osteogenic differentiation of human mesenchymal stem cells (hMSCs) for improved bone regeneration through metabonegenic regulation.^[41,42]

To address the limitations of the current bone wax/putty, herein, a new generation of biodegradable citrate-based osteopromotive bone putty was developed by compositing a BPLP polymer synthesized by reacting citric acid (CA), 1,8-octanediol (OD), and L-Serine (Ser) with HA, referred to as BPLP-Ser/HA putty. BPLP-Ser/HA is malleable and can press-fit into irregular defects easily with comparable handling properties to bone wax. BPLP-Ser/HA was characterized via its compression strength, adhesion strength, sealing capability, swelling, hemostatic effects, pH change, and mass loss. BPLP-Ser/HA was cultured against mouse fibroblast cells (L929) to evaluate its cytocompatibility in vitro. Finally, a cranial bone defect rat model was used to evaluate the osteopromotive effects of BPLP-Ser/HA in vivo with a commercial bone wax as control.^[43]

2. Results and Discussion

2.1. Intrinsically Biomimetic and Multifunctional BPLP-Ser/HA Putty is Prepared Through a Cost-Effective One-Step Synthesis

Motivated by the complex hierarchical structure of bone, consisting of 60–65 wt% HA intimately associated with an organic collagen and proteinaceous matrix, significant effort has been expended developing effective inorganic/organic composites to potentiate bone regeneration. While organic biomaterials including gelatin,^[44,45] chitosan,^[46] hyaluronic acid, collagen,^[47] and alginate as well as synthetic polymers such as poly(lactic acid) (PLA), poly(glycolic acid) (PGA), poly(propylene fumarate) (PPF), and poly(caprolactone) (PCL) have been extensively studied, successful incorporation of biomimetic levels of ceramic has remained elusive, with significant instances of phase separation, brittleness and mechanical failure, and poor in vivo integration and regeneration.^[24,48–52] Modification strategies to one or both phases, such as conjugation of

ceramic binding groups to polymer chains or surface modification of ceramics with lactic acid oligomers,^[53] isocyanates,^[54] poly(amino acids), catechols,^[52,55] or silanes have resulted in enhanced physical properties; however, such processes are inherently limited due to the low reactivity of ceramic surface groups and increase both cost and complexity, motivating the search for composite systems with inherent biomimetic structures.^[52,56]

Citrate has emerged as a critical structural component of native bone, comprising 5% by weight and covering 1/6 of the inorganic bone surface, strongly associating with both the fibrous collagen organic phase and amorphous calcium phosphate (ACP) inorganic phase during bone formation, decreasing surface binding energy between the two phases and facilitating intra- and interfibrillar mineralization.^[56–58] Further, binding of citrate to specific surfaces of HA as it undergoes crystallization from early amorphous phases serves to regulate crystal size/shape to the preferred nanocrystal morphology, preventing bulk crystal fusion and brittle mechanics.^[58–61] Inspired by the dual-phase bridging roles of *in vivo* soluble citrate, we theorized that polymers directly incorporating citrate could intrinsically recapitulate the strong organic/inorganic phase binding in a biomaterial platform.

BPLP-Ser prepolymer was duly synthesized (**Figure 1a**) via a simple, cost-effective, catalyst-free polycondensation reaction between: 1) a tetrafunctional citrate moiety enabling covalent crosslinking and ceramic chelation; 2) the naturally occurring amino acid L-Serine, enabling the formation of a previously described dioxo-pyridine ring (DPR) fluorophore with high quantum yield, excellent photostability, and tunable fluorescence emission (up to 725 nm),^[62] and 3) difunctional 1,8-octanediol as an alkyl chain moiety, as a viscous low molecular weight oligomer. Utilizing the calcium chelating potential of the abundant free carboxyl and hydroxyl groups in BPLP-Ser oligomers, we next directly mixed their ethanolic solutions with HA to obtain BPLP-Ser/HA composites, maintaining excellent homogeneity, pliability, and putty-like consistency after solvent evaporation even when HA concentration reached 65 wt% (**Figure 1b**). Scanning electron microscopy (SEM) and energy dispersive X-ray spectroscopy (EDS) analysis (**Figures S1 and S2**, Supporting Information) confirmed successful integration of the ceramic phase, displaying relatively smoother and more continuous surfaces compared to commercial bone wax, well-distributed HA particles uniformly incorporated within the bulk material and uniform calcium and phosphate distributions. **Figure 1b** further demonstrated that BPLP-Ser/HA putty is malleable and can be molded into complex structures via press-fit into various molds. BPLP-Ser/HA displayed the strong band-shifting fluorescence (330 – 725 nm) (**Figure 1d**) inherent to the excitation-dependent dioxo-pyridine (DPR) moiety and strong, visible green emission (580 nm) (**Figure 1c**). Thus, we successfully leveraged citrate's unique chemistry into a branched, highly carboxylated mimic of the collagenous bone template, enabling intrinsic organic/inorganic binding and homogenization, replicating the phase composition and interaction of native bone, as a malleable press-fit putty. Further, reaction of citrate with L-Serine results in inherent material fluorescence sans utilization of toxic dyes or quantum dots, beneficial in assessing material residuals or material degradation

through fluorescence imaging *in vivo* or during histological analyses. Critically for clinical use, BPLP-Ser/HA represents a stable, off-the-shelf material capable of instant use without the need for complex mixing, toxic crosslinking agents, defined working times, or hazardous reaction conditions (free radicals, oxidizers, exothermia) that define commonly used injectable/moldable products including CPCs, hydrogels, and poly(methyl methacrylates) (PMMA).

2.2. BPLP-Ser/HA Putty Displays Mechanics Comparable to Early Nonmineralized Bone and Mechanical Stability in Hydrated Conditions

Bone's primary role as a highly mineralized support structure has seen traditional implants designed to replicate the high mechanics of the mature tissue (compressive stress $\approx 100 - 230$ MPa, modulus $\approx 7 - 30$ GPa).^[63] Indeed, canonically, putty-like citrate-based polymer/HA composites have been crosslinked under prolonged and harsh thermal conditions to achieve similar values; however, such processing precludes their use in irregular defects.^[51,63] Contrary to its final properties, the initial stages of osteogenesis consist of cell-mediated reorganization and mineralization of a cartilage intermediate or mesenchyme in endochondral ossification and intramembranous ossification, respectively, moving through fibrous and cartilaginous soft tissues to woven and lamellar mature bone.^[64] Challenging traditional implant ideology, recent research has suggested that softer implants are better capable of replicating the dynamic properties of healing bone, optimizing the transfer of mechanical properties to cells, and initiating a cascade of mechanosensitive signals necessary for endogenous healing.^[65] We, therefore, theorized that the hitherto underutilized putty-like intermediate stage of BPLP-Ser/HA could not only enable the desired press-fit application, but attain mechanical properties comparable to the earliest stages of bone.

Accordingly, the compressive mechanical properties of BPLP-Ser/HA putties were assessed. Compressive strength and initial modulus of putties increased proportionally to HA content (**Figure 2**). The incorporation of 55 wt% HA (409.51 ± 30.25 kPa) significantly improved the compressive strength as compared to the putties with 40 wt% (1.95 ± 0.69 kPa), 45 wt% (56.11 ± 4.97 kPa), and 50 wt% HA (116.67 ± 777 kPa) in dry conditions (**Figure 2a**), reinforcing the role of HA both as macro-crosslinker via the multiple strong binding interactions with the BPLP-Ser polymer and as a high strength ceramic material. Similarly, the initial modulus also significantly increased as the concentration of HA was increased (1.08 ± 0.36 , 67.1 ± 4.69 , 99.49 ± 18.91 , and 427.22 ± 84.98 kPa for 40, 45, 50, and 55 wt% HA) (**Figure 2b**). Interestingly, in contrast to most biomaterials, the compressive strength of the putties increased under wet conditions, which is beneficial for *in vivo* applications. The compressive strength for the putty with 45%, 50%, and 55 wt% HA significantly increased to 91.22 ± 7.33 , 285.69 ± 30.35 , and 764.80 ± 60.61 kPa, respectively, following submersion in phosphate-buffered saline (PBS) at 37 °C for 24 h. In contrast, putty containing 40 wt% HA lost mechanical stability, elucidating the importance of sufficient inorganic content to material cohesion and highlighting the physio-mechanical

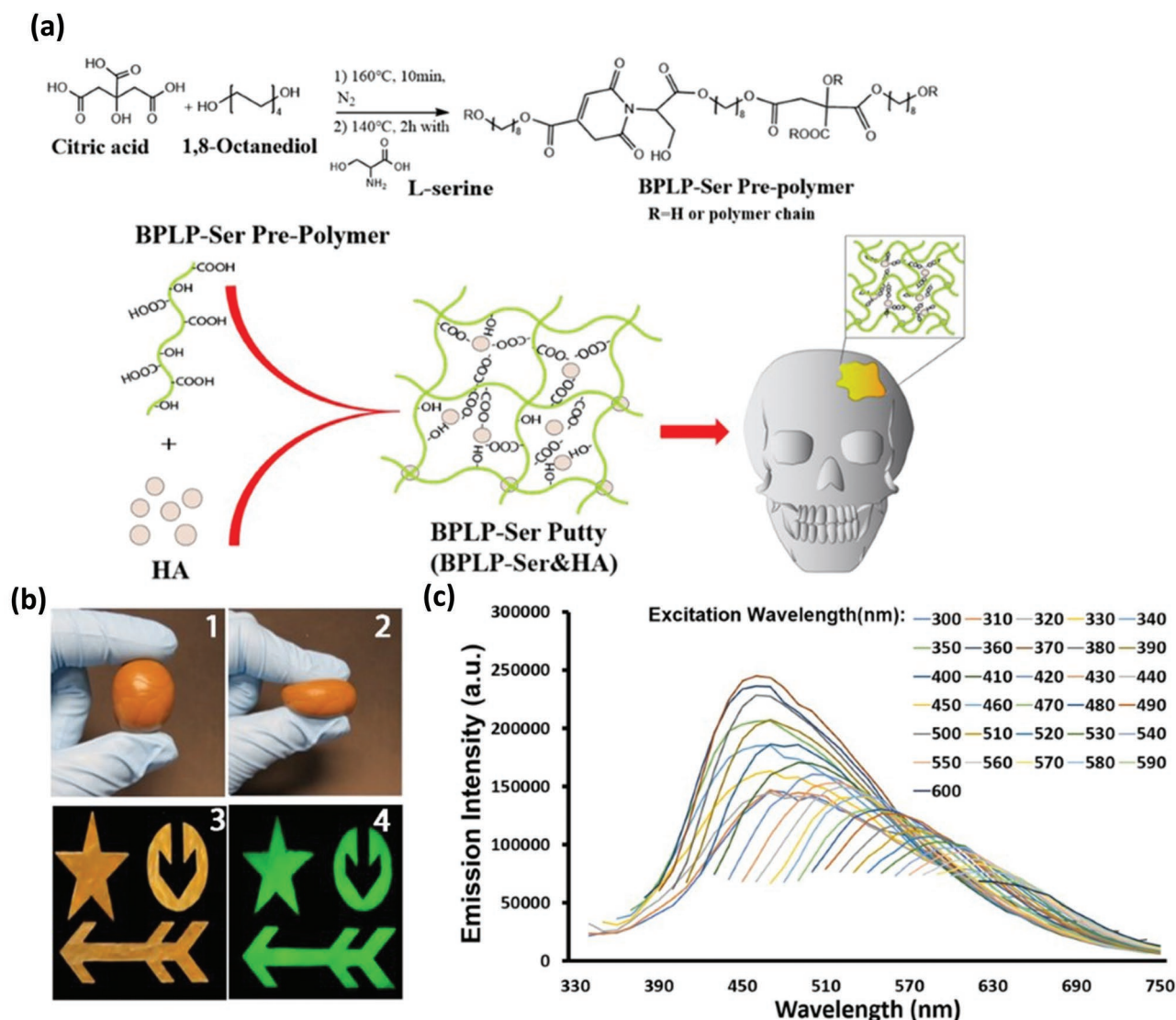


Figure 1. Design of multi-functional BPLP-Ser/HA bone putty. a) Schematic demonstration showing the synthesis of BPLP-Ser, fabrication of citrate-based fluorescent composites (BPLP-Ser/HA), and press-fit into irregular cranial defects. b) BPLP-Ser/65%HA putty (1) is highly malleable and can be molded in different shapes (2 and 3) while displaying excellent fluorescent emission (580 nm) (4). c) Emission spectra of BPLP-Ser/50%HA putty under excitation from 330–600 nm, demonstrating excitation-dependent fluorescent emission.

advantages of the BPLP-Ser/HA putty versus pure BPLP-Ser in vivo. While the same trend was observed in the initial modulus, the differences between the dry and wet mechanics were not significant (Figure 2b). The strength of conventional bone wax was significantly lower than the BPLP-Ser/HA putty with 50% and 55% HA and similar to the 45% HA formulation under both dry and wet conditions; however, the initial modulus was much greater (49.98 ± 5.57 MPa and 59.19 ± 5.70 MPa in dry and wet conditions, respectively). Additionally, we also observed an increase in initial modulus under wet conditions compared to the dry condition, consistent with the putty. While the underlying mechanism of the increased wet mechanical properties of BPLP-Ser/HA putty is not entirely clear, we reasoned that: 1) the absorption of PBS by the putty helps ionize carboxyl groups in the BPLP-Ser polymers which can better chelate with calcium-containing HA particles, and 2) defined hydrophobic

(diol) and hydrophilic (citrate) regions within BPLP-Ser polymers preferentially reorient in a bulk nonsolvent (in this case aqueous PBS), increasing material density and thus mechanics, concurrent with results observed in diverse materials including poly(HEMA) hydrogels and poly(ethylene glycol) (PEG)-poly(lactide-co-glycolide) (PLGA) block polymers.^[67] Further, previous formulations of thermally crosslinked citrate-based materials incorporating long-chain hydrophobic diols revealed the formation of distinct hydrophobic association regions, lending shape memory properties and increased mechanics under extended wet conditions.^[68] To further elucidate the relative contribution of the two above effects, mechanics were next tested following hydration in deionized (DI) water, revealing a further increase in strength (126.64 ± 10.45 , 147.04 ± 13.10 , 338.19 ± 20.87 , and 1134.29 ± 105.02 kPa for Bone Wax, and BPLP-Ser putty with 45, 50, and 55%HA, respectively) as

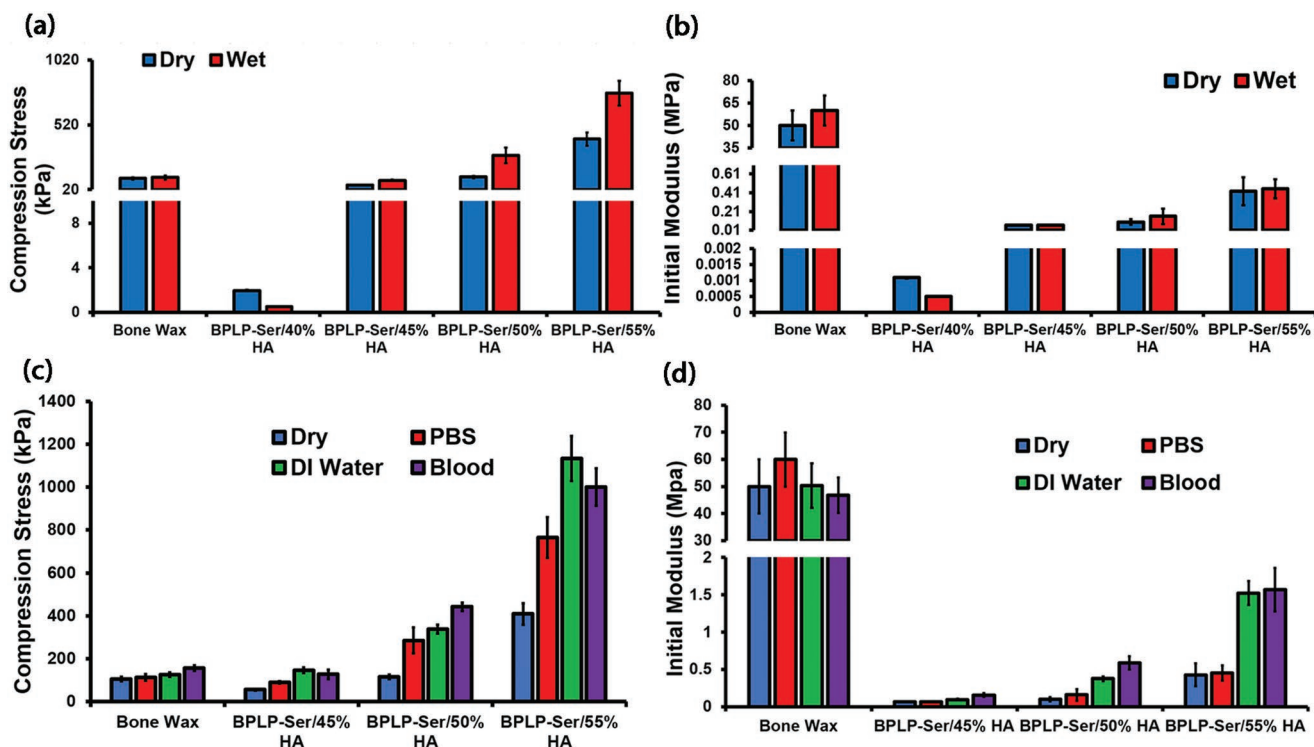


Figure 2. Mechanical properties of commercial Bone Wax and BPLP-Ser/HA putty. a) Peak stress and b) Initial modulus of Bone Wax and BPLP-Ser putty with 40%, 45%, 50%, and 55% HA when compressed to 50% strain in dry and wet (24 h in 1x PBS) conditions. c) Peak stress and d) Initial modulus of the wet-conditioned (24 h in 1x PBS, DI water, or bovine whole blood) Bone Wax and BPLP-Ser putty with 45%, 50%, and 55% HA when compressed to 50% strain, $n \geq 5$.

well as initial modulus (95.19 ± 10.35 , 375.86 ± 30.92 , and 1000.73 ± 876.2 kPa for putty with 45%, 50%, and 55%HA (modulus of Bone Wax, in contrast, was similar to the PBS value, reaching 50.29 ± 8.12 MPa)) (Figure 2c,d). In light of the above results and given the relative polymer chain freedom in BPLP-Ser/HA putties crosslinked by chelation only, it can be posited that in response to the nonsolvent PBS and DI water, diol regions are capable of such reorientation (such reorientation of long hydrophobic chains could also explain the increased wet mechanics of commercial bone wax, which lacks both significant ionizable groups and HA) and that this effect is dominant in comparison to ionization of carboxylates (additionally, phosphate anions present in PBS may interfere with carboxylate-HA interactions, counteracting this benefit). Finally, incubation in whole blood resulted in similar or increased strengths (156.13 ± 13.07 , 127.91 ± 22.40 , 442.22 ± 19.23 , and 1000.73 ± 876.2 kPa) and moduli (46.77 ± 6.51 MPa and 156.70 ± 24.17 , 586.32 ± 90.56 , and $1,567.42 \pm 292.50$ kPa) compared to DI water (Figure 2c,d). Tellingly, a well-defined layer of coagulated blood was observed on the surface of all BPLP-Ser putty formulations that was absent from Bone Wax, indicating significant interactions between the putty surface and blood cells/proteins. Given the large calcium content inherent to BPLP composites, it can be inferred that calcium cations within the bulk material or released into the local environment are capable of mediating clotting and further that the resulting crosslinked protein network is capable of interacting with and mechanically reinforcing the material. Strong inter-

facial binding between the inorganic BPLP-Ser polymer phase and HA inorganic phase, with HA particles acting as macro-crosslinker and calcium reservoir, thus resulted in a material with tunable mechanics achieving both comparable handleability to bone wax, critical to its application, and similar mechanics to materials promoting osteogenic differentiation (modulus ≈ 15 kPa – 30 MPa), further reinforcing BPLP-Ser/HA as a biomimetic platform, with significant hydration induced strengthening in physiological conditions, beneficial to sealing and reinforcement of fractured and bleeding bone in vivo.^[69,70]

2.3. BPLP-Ser/HA Putty Achieves Tunable Degradation Rates and Swelling Ratios while Maintaining Material Stability

Proper material degradation rate is critical to ensure effective bone regeneration, with rapid degradation leading to inability to properly stabilize defects and allow time for new tissue formation, while extended degradation conversely prevents tissue ingrowth, delaying proper defect healing. Traditional thermally cross-linked citrate-based composites display long degradation times (10 to 20 wt% in 1 year);^[51] however, we posited that by utilizing BPLP-Ser/HA putty containing only ionic and chelation bonds, an intermediate degradation rate (months) could be achieved (as opposed to pure BPLP oligomers with rapid degradation rates of ≈ 2 weeks).^[70] Verification of degradation mass loss was thus performed (Figure 3a). Interestingly, HA concentration did not significantly influence the degradation

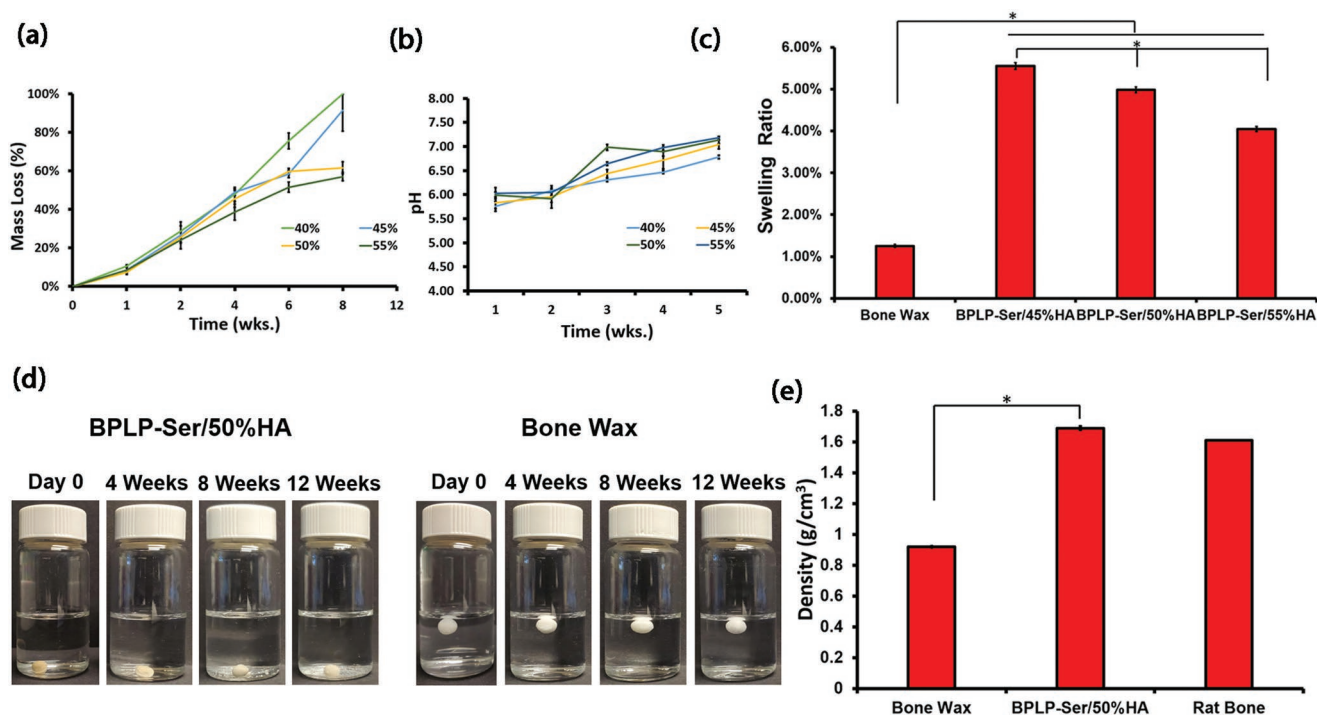


Figure 3. Physical characterization of BPLP-Ser/HA putty. a) Mass loss of BPLP-Ser/HA putty over 8 weeks. b) pH evolution of BPLP-Ser/HA putty degradation media within 5 weeks. c) swelling ratios of bone wax and BPLP-Ser/HA putty after 24 h immersion in 1xPBS. d) Stability of Bone Wax and BPLP-Ser/50%HA in 1x PBS over 12 weeks. e) Density of Bone Wax, BPLP-Ser/50% HA putty, and rat calvarial bone. * $p < 0.05$, $n \geq 6$ except for (c) ($n \geq 3$).

rate of the putty within the first 4 weeks. It wasn't until week 6 that BPLP-Ser putty synthesized with the least amount of HA (40 wt%) showed a significantly higher mass loss of $75.58 \pm 4.17\%$, whereas all other formulations had approximately half their mass remaining; however, at 8 weeks BPLP-Ser/40% HA was completely degraded while the average mass loss of BPLP-Ser/45% HA was $97.37 \pm 2.10\%$. In contrast, BPLP-Ser/50% HA and BPLP-Ser/55% HA exhibited an average of nearly 60% mass loss at 8 weeks, again reinforcing the role of HA as a composite crosslinker (as well as a more hydrophobic and stable component), with increased HA leading to longer degradation times. Concomitant evaluation of degradation pH revealed a sharp decrease to acidic values (<7) within the first 2 weeks, gradually recovering by the 3rd week and remaining stable thereafter (Figure 3b). Similar to mass loss, no significant difference was observed between HA concentrations at each time point. While such initial pH drops may be of concern in vitro, it should be considered that: 1) the initial stages of bone remodeling post fracture involve the activation of large populations of osteoclasts which subsequently excrete acid locally to initiate dissolution of the ceramic bone phase, liberate necessary constituent minerals, and activate growth factors such as transforming growth factor-beta (TGF- β), thus a locally temporary acidic microenvironment is a necessary component of healing^[64,71]; 2) rates of clearance of degradation products in vivo are enhanced due to active uptake by cells as well as diffusion into local vasculature, and 3) the primary mediator of pH drop in BPLP-Ser/HA materials, citrate, is a necessary metabolite whose cellular uptake is upregulated in differentiating osteoblasts, leading to its rapid local uptake.^[42] Therefore, rather than

a potential concern, the release of acidic citrate could function to better mimic local conditions and cellular needs in vivo.

The high swelling ratios of many injectable polymeric systems (such as hydrogels which can swell 100% or even 1000%),^[73] potentially causing post-operative pain, pressure-induced damage to peri-defect tissues (particularly in the brain and spinal regions), and potential implant dislodgement, lead to reduced patient satisfaction and impaired healing. Swelling ratios of BPLP-Ser/HA putties in PBS were thus compared along with commercial bone wax (Figure 3c). Significantly different swelling ratios of 5.55 ± 0.12 , 4.98 ± 0.06 , and $4.05 \pm 0.09\%$ were obtained for BPLP-Ser/45% HA, BPLP-Ser/50% HA, and BPLP-Ser/55% HA, respectively, while bone wax displayed a swelling ratio of $1.25 \pm 0.03\%$, significantly lower than all BPLP-Ser/HA formulations, expected due to the higher hydrophobicity of the pure alkyl chain wax relative to BPLP-Ser/HA. Nonetheless, BPLP-Ser/HA composites demonstrated an advantageous, low swelling character. In line with their minimal swelling ratios and extended degradation times, BPLP-Ser/50% HA composites demonstrated significant bulk stability in vitro, maintaining their initial dimensions sans noticeable swelling or significant fragmentation even after 12 weeks, suggesting that residual organic/inorganic crosslinks maintain a stable network even after significant bulk mass loss ($>60\%$) (Figure 3d). Stability assessment also served to highlight the significant difference in material density between BPLP-Ser/HA and bone wax (Figure 3e). BPLP-Ser/50% HA displayed a density of (1.69 g cm^{-3}) , comparable to explanted rat calvarial bone (1.61 g cm^{-3}) and matching literature values for human bone ($1.62\text{--}1.92 \text{ g cm}^{-3}$),^[74] further confirming the biomimetic

nature of BPLP-Ser/HA. In contrast, bone wax had a significantly lower density (0.92 g cm^{-3}), enabling its buoyancy in PBS (leading to an increased likelihood of extravasation of small particles through local vasculature) (Figure 3d). In sum, physical characterization of BPLP-Ser/HA putty revealed significantly tunable properties through control of material composition, achieving degradation rates intermediate between the ultra-rapid degradation of current biodegradable bone waxes such as Ostene (1–2 days) and the lengthy degradation or nondegradability of CPC cements and PMMAs, respectively, enabling functionality both as acute fracture sealing agents and support for tissue regeneration. Further, effective polymer/HA interactions and high HA loading capability resulted in low swelling ratios, effective material stability, and increased material density, reducing the likelihood of material failure, dislodgement, and extravasation compared to nondegradable bone waxes (an additional benefit of degradability being the eventual dissolution of dislodged particles in vivo).

2.4. BPLP-Ser/HA Putty Achieves Hemostatic and Adhesive Properties

Rapid and effective bleeding control is necessary in multiple orthopedic surgeries as well as a number of other surgeries requiring a bone incision. Commercial bone wax enables clot formation via infiltration and physical occlusion of blood vessels, known as the tamponade effect.^[75,76] We reasoned that BPLP-Ser/HA, by virtue of its malleable initial character combined with excellent stability and hydration induced strengthening capabilities, would perform capably as a tamponade material and further that calcium release would actively enhance blood clotting, as discussed in Section 2.2. Hemolysis was first assessed to determine the effect of materials on erythrocytes, revealing significantly higher lysis (23.64 ± 0.62 , 25.05 ± 0.77 , and $24.71 \pm 2.23\%$ for BPLP-Ser with 45, 50, and 55%) in the presence of putty versus Bone Wax ($1.16 \pm 0.15\%$) (Figure 4a), likely due to local pH drop and release of calcium cations, both known mediators of erythrocyte cell membrane disruption (the latter particularly attested to in response to silver cations);^[77,78] however, it should be considered both that these values are within the range of other hemostatic materials and that BPLP-Ser putty is not designed for prolonged blood contact (indeed being sealed off from active blood flow by clotting), reducing the effect of hemolysis beyond the acute stage.^[79–81] Whole blood clotting time was next assessed, demonstrating a significant decrease in clotting time for all BPLP-Ser putty formulations compared to control and Bone Wax (12.33 ± 0.26 , 11.75 ± 0.69 , and $11.33 \pm 0.41 \text{ min}$ for 45%, 50%, and 55% HA versus 14.92 ± 0.38 and $14.75 \pm 0.52 \text{ min}$ for control and Bone Wax) (Figure 4b), confirming the capability of putty to promote clotting, acting as an active hemostat in comparison to Bone Wax and demonstrating a reduction in clotting time ($\approx 17\%$, 21% , and 24%) comparable to other solid hemostats.^[80] The sealing potential of BPLP-Ser/HA putties and commercial bone wax was evaluated using the previously described liquid sealing test with modifications (Figure 4c).^[82] Briefly, a gravity-induced pressure head equivalent to physiological blood pressure in amputated medullary cavities (140 mmHg)^[76] was established

by filling a 2 m vertical polypropylene tube sited within a $37 \text{ }^\circ\text{C}$ incubator with blue dye. A defined amount of sealant material was then compressed by hand within the bottom tube opening, forming the initial plug seal. The lower end of the tube was finally placed within a beaker containing clear PBS, simulating wet physiological conditions and enabling easy leakage detection. BPLP-Ser/45% HA failed most rapidly ($<20 \text{ min}$), due to its relatively weak mechanics, while commercial Bone Wax occluded flow for 2 h (Figure 4d) followed by failure. In contrast, BPLP-Ser/50% HA and BPLP-Ser/55% HA withstood physiological pressure for 24 h, significantly longer than bone wax and the typical in vivo clotting time ($8\text{--}15 \text{ min}$),^[83] which could be beneficial in cases of compromised clotting or clot dislodgement during or post-surgery. In vitro sealing thus confirmed the favorable performance of BPLP-Ser/HA as tamponade material while highlighting the importance of a high HA loading.

Effective blood vessel occlusion in the bone environment additionally requires the ability to successfully adhere to and infiltrate the porous native bone surface. In light of the demonstrated ability of BPLP-Ser to bind HA, the chemical structure of BPLP-Ser, including free carboxyl and hydroxyl groups, is expected to bind strongly with the bone tissues through hydrogen bonds, hydrophobic interactions, and ionic interactions, in contrast to commercial Bone Wax and PMMAs, which depend predominantly on mechanical interlock rather than active binding moieties.^[84,85] As shown in Figure 4e, adhesion strengths to a trabecular bone of putty formulations were higher than Bone Wax (399.74 ± 43.49 , 366.27 ± 42.99 , and $557.35 \pm 17.04 \text{ kPa}$ for 45, 50, and 55%HA versus $187.57 \pm 4.57 \text{ kPa}$ for Bone Wax) as well as meeting or exceeding values obtained for CPCs, PMMA, and hydrogel-based sealants.^[17] Enhanced adhesion of BPLP-Ser/50% HA versus bone wax was further demonstrated via a femoral condyle reattachment model utilizing chicken tissue, in which BPLP-Ser/50% HA was able to bond strong enough to support the weight of the complete chicken leg while bone wax failed (Figure 4f). BPLP-Ser/50% HA also demonstrated the ability to seal the femoral intramedullary cavity of wet chicken tissue (amputation model) (Figure S3, Supporting Information) comparable to bone wax. BPLP-Ser/HA thus demonstrated potential in promoting clotting, resisting blood pressure, and enabling wet tissue adhesion.

2.5. BPLP-Ser/HA is an Intrinsically Antimicrobial Biomaterial

Surgical and implant-associated infection is a common occurrence, leading to inflammation, pain, impaired healing, and tissue necrosis, necessitating development of effective antimicrobial biomaterials. While various modification strategies have been adopted to confer antimicrobial properties to polymers, including the introduction of quaternary ammonium salts and antimicrobial peptides into the polymers, incorporation of antimicrobial ions such as copper, silver, and zinc, and encapsulation or conjugation of antimicrobial drugs such as gentamycin are common, materials demonstrating inherent antimicrobial potential offer attractive alternatives in terms of lower material complexity and cost.^[85–87] Soluble citrate functions as a potent antimicrobial

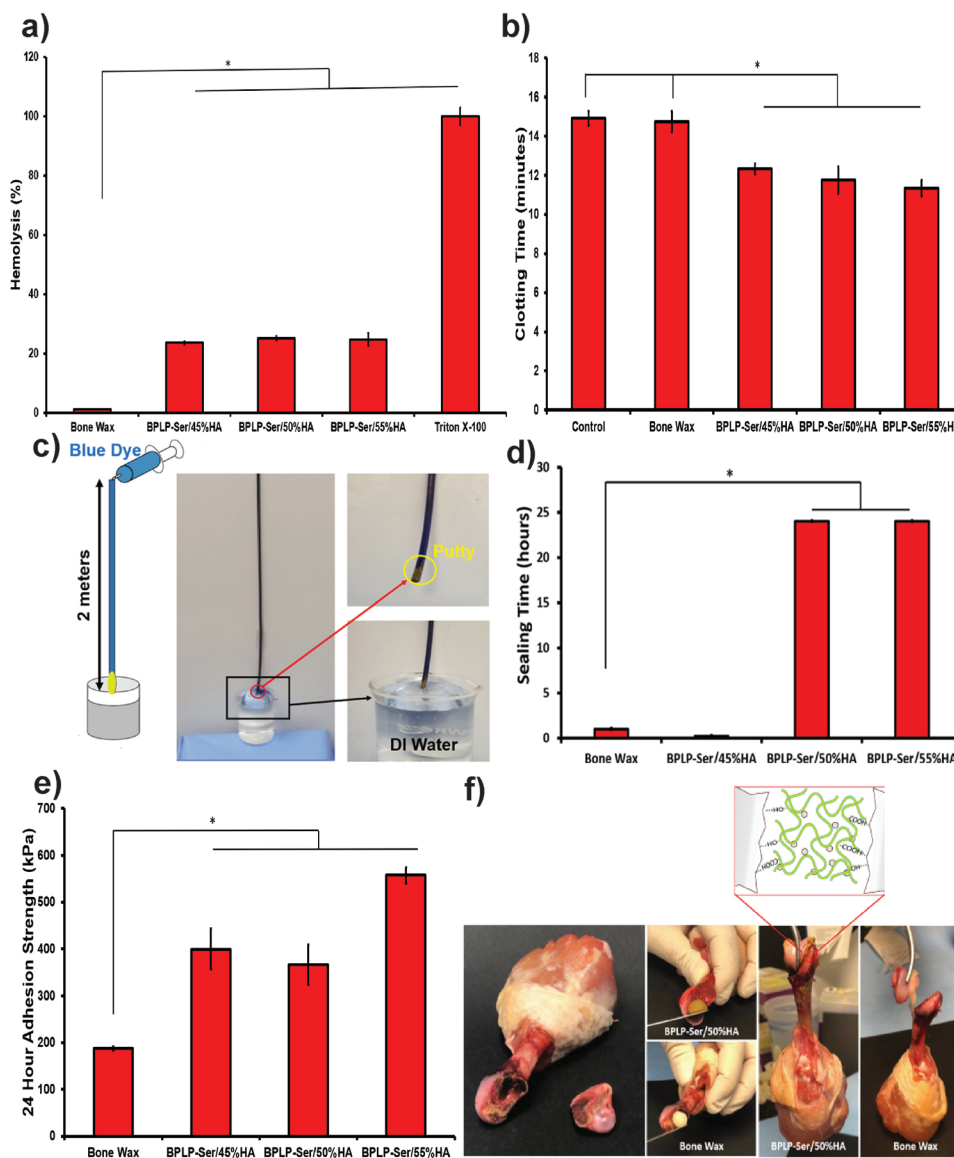


Figure 4. Liquid sealing and adhesion tests of BPLP-Ser/HA putty. a) Hemolytic properties of Bone Wax and BPLP-Ser/HA putty. b) Whole blood clotting time of Bone Wax and BPLP-Ser/HA putty. c) Schematic demonstration and photographs of sealing experiments at 37 °C; a two-meter tube was placed vertically against the wall, then blue dye was injected through the upper end of the tube to simulate physiological blood pressure. The lower end of the tube was plugged with Bone Wax or BPLP-Ser/HA putty after which the lower tube end was immersed in DI water, wetting the materials from the outside. d) Liquid sealing time of Bone Wax and BPLP-Ser/HA putty at 37 °C. e) Adhesion strength of Bone Wax and BPLP-Ser/HA putty to the trabecular bone after 24 h in PBS. f) In vitro adhesion of separated femoral condyle and femur via Bone Wax and BPLP-Ser/50%HA putty and illustration of a proposed mechanism for the adhesive property of BPLP-Ser/HA putty. * $p < 0.05$, $n \geq 3$.

agent, utilized in multiple germicidal formulations, dental rinses, and agricultural bactericides.^[88] Citrate is thought to inhibit bacteria via lowering of intercellular pH, inducing DNA, protein, and membrane damage as well as inhibiting nicotinamide adenine dinucleotide (NADH) oxidation, leading to cell death, as well as through direct, disruptive binding to cell membranes and chelation of calcium and magnesium cations required for cellular function and growth.^[37,88] Accordingly, citrate-based materials have uniformly displayed antimicrobial function dependent on relative citrate content and degree of crosslinking.^[37] It was therefore expected that BPLP-Ser/HA putties, being minimally crosslinked and

mediating a pronounced acute pH drop in vitro as described in Section 2.3, would be excellent candidates as intrinsically antimicrobial composites. Accordingly, BPLP-Ser/HA putty was tested against *Staphylococcus aureus* (*S. aureus*) and *Escherichia coli* (*E. coli*) with an initial bacterial concentration of 1×10^6 CFU ml⁻¹ as representative Gram-positive and Gram-negative species with bone wax serving as control. As shown in Figure 4a,b, optical densities of *E. coli* and *S. aureus* treated with BPLP-Ser/45% HA, 50% HA, and 55% HA were significantly decreased compared to both positive and Bone Wax controls following 24 h of incubation, while no significant difference was observed between putty formulations, illustrating the minimal impact of

HA content. All BPLP-Ser/HA formulations exhibited better performance against *S. aureus* compared to *E. coli*, with the optical densities of the former diminished to a level similar to pure media. BPLP-Ser/HA and bone wax displayed inhibition ratios between 50%–55% and 25% against *E. coli*, respectively (Figure 4c), while the inhibition ratios of BPLP-Ser/HA against *S. aureus* were nearly 100% (Figure 4d). In contrast, Bone Wax displayed negative performance. BPLP-Ser/HA putties represent a novel class of antimicrobials via effective citrate release, in stark contrast to commercial bone waxes and many other moldable/injectable materials which require modification with or loading of distinct antimicrobial agents, facilitating effective prevention and treatment of infection.

2.6. BPLP-Ser/HA Displays Biocompatibility and Osteopromotion

Biocompatibility of BPLP-Ser/45% HA, 50% HA, and 55% HA degradation products was assessed via CCK-8 assay against L929 cells (Figure 5a) with PLGA 75:25 as control. At the highest concentration (1x), cell viabilities of BPLP-Ser/HA formulation treated cells were significantly lower (<5%) compared to PLGA (~60%), while cell viabilities increased with decreasing degradation product concentration. At 5x dilution, cell viabilities of BPLP-Ser/45% HA and BPLP-Ser/50% HA groups increased to (~60%), whereas cell viability in the BPLP-Ser/55%

HA group reached ~80%, equivalent to PLGA. Further, at 10x and 100x dilutions, cell viabilities in all groups were equivalent, displaying minimal toxicity. The effects of BPLP-Ser/45% HA, 50% HA, and 55% HA degradation products on cell proliferation were also studied, again utilizing PLGA as control (Figure 5b). Cell numbers uniformly increased from Day 1 to Day 3 and from Day 3 to Day 5, while microscopy revealed increased numbers of adherent cells displaying normal spread morphology (Figure S4, Supporting Information). Cell viabilities of each group exposed to 10x, 50x, and 100x diluted products after 3 days were similar, corresponding to the trends in cytotoxicity, while on Day 5, cell numbers in the groups treated with 50x and 100x diluted degradation products of BPLP-Ser/HA were significantly higher than both untreated and PLGA controls. These results suggest that degradation products of BPLP-Ser/HA putties are not significantly toxic to cells except at the highest concentration (which given the prolonged degradation period of BPLP-Ser/HA and significant in vivo clearance is not expected to be attained under physiological conditions) and that less concentrated products in fact promote cell proliferation, in line with previous citrate-based materials and constituent monomers.^[90] Additionally, direct seeding of hMSCs on BPLP-Ser/50%HA resulted in successful proliferation (Figure S5, Supporting Information). While cell growth was initially limited ($111.76 \pm 1.87\%$ on Day 3), likely due to pH change and leaching of soluble products from the bulk material, cell numbers more than doubled by Day 7 ($247.27 \pm 7.02\%$) and increased more

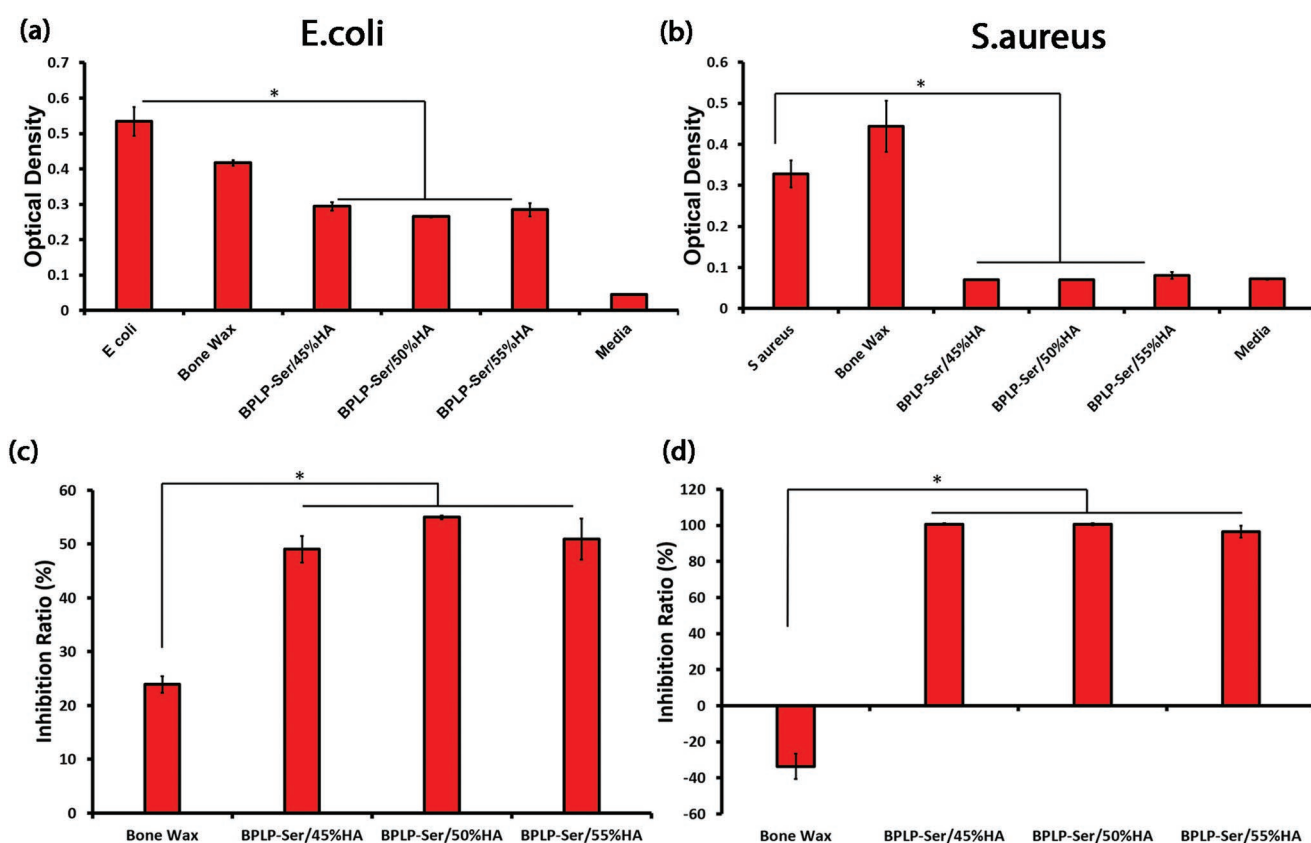


Figure 5. In vitro antibacterial effects of BPLP-Ser/HA putty. Optical density of *E. coli* (a) and *S. aureus* (b) incubation broth with and without the addition of Bone Wax and BPLP-Ser/HA putties. Inhibition ratios against *E. coli* (c) and *S. aureus* (d) of Bone Wax and BPLP-Ser/HA putty for 24h. * $p < 0.05$, $n \geq 4$.

than 10-fold by Day 14 ($110735 \pm 48.25\%$) when compared to Day 1, indicating that while BPLP-Ser/HA may present a challenging cellular environment in the acute phase, it is capable of supporting significant cell growth.

Osteogenic capability is a critical benchmark in the transition from inert to bioactive bone implants. Citrate, long recognized as a critical structural component of bone, has more recently been implicated as a critical bioactive factor in osteogenesis.^[91,92] Our previous research identified citrate as a key osteopromotive factor, mediating osteogenic differentiation through uptake of soluble citrate by the solute carrier family 13, member 5 (SLC13a5) channel and subsequent regulation of metabolic pathways centered on the canonical tricarboxylic acid (TCA) cycle, fueling the high energy demands of differentiating hMSCs and promoting downstream osteogenic processes (termed the metabonegenic effect).^[41,42] We, therefore, assessed the osteogenic differentiation of hMSCs in the presence of osteogenic media containing 50x and 100x diluted BPLP-Ser/HA degradation products via expression of alkaline phosphatase (ALP) and calcium deposition with pure osteogenic media (OG) as control (Figure 6c). ALP levels were similar for all groups on Day 7, while on Day 14 ALP levels for BPLP-Ser/45% HA, BPLP-Ser/50% HA, and BPLP-Ser/55% HA at both 50x and 100x dilution were lower than the OG control; however, ALP

levels for all BPLP-Ser/HA groups increased significantly from Day 7 to Day 14, indicating successful osteogenic differentiation. Further, hMSCs exposed to BPLP-Ser/HA uniformly displayed calcium nodule formation on Day 14 with no significant difference observed between BPLP-Ser/HA groups and OG control, indicating successful mineralization in the presence of degradation products (Figure 6d). These results support the osteopromotive effect of BPLP-Ser/HA derived citrate, in line with previous in vitro and in vivo studies.^[41,93]

2.7. BPLP-Ser/HA Putty Promotes Cranial Bone Regeneration Equivalent to Autograft

Positive in vitro results as outlined above motivated in vivo testing of BPLP-Ser/50% HA (chosen to balance material handling, degradation, and bioactive properties) against negative (NC-) and positive (autograft) controls as well as commercial Bone Wax in a critical-sized full-thickness cranial defect rat model. Cranial defects were chosen due to their well-known reduced healing response, a function of poor blood supply and deficiency of bone marrow sources (thus representing a severe defect model), as a commonly occurring and easily accessible irregular defect well suited to press-fit materials, and as a

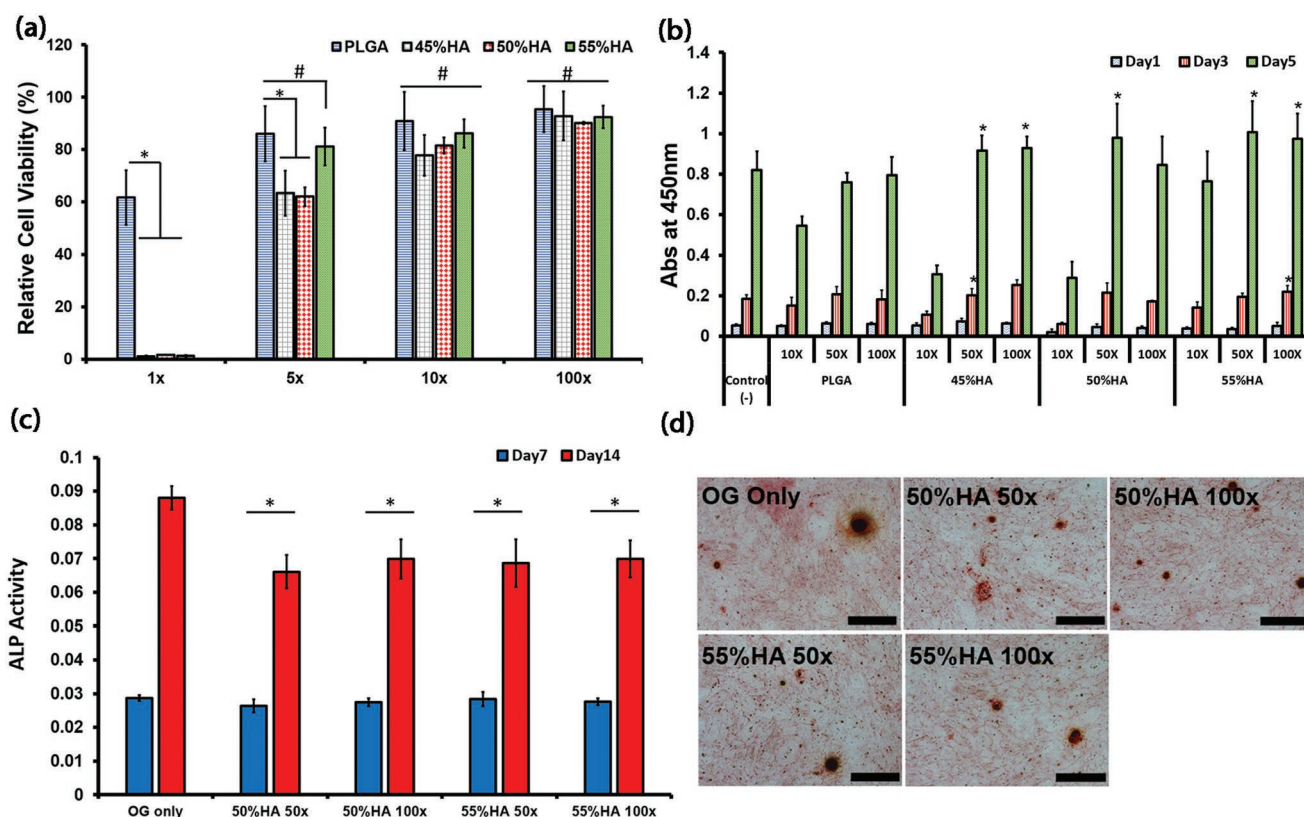


Figure 6. In vitro cytotoxicity, proliferation, and osteogenic capability of BPLP-Ser/HA putty. a) 24h cytotoxicity of degradation products of PLGA and BPLP-Ser/HA putty at 1x, 5x, 10x, and 100x dilution factors against L929 cells. b) Cell proliferation of L929 cells in the presence of degradation products at 10x, 50x, and 100x dilution factors. c) ALP production of human mesenchymal stem cells (hMSCs) cultured in OG medium and OG medium containing degradation products of BPLP-Ser/HA putty at 50x and 100x dilution factors. d) Calcium deposition of hMSCs cultured in OG medium and BPLP-Ser/50%HA and OG medium containing BPLP-Ser/55%HA degradation products at 50x and 100x dilution factors, scale bar = 500 μm. * $p < 0.05$, # $p > 0.05$, $n \geq 3$.

defect in which Bone Wax is commonly utilized (particularly in cases of neural procedures).^[94,95] 8 mm cranial defects were created, resulting in significant bleeding (Figures S6c–e, Supporting Information), followed by application of the appropriate material (preventing further bleeding in the case of BPLP-Ser/50%HA and Bone Wax (Figures S6f and S7a,b, Supporting Information) (detailed surgical procedure provided in Experimental Section and Figures S6 and S7, Supporting Information) and wound closure.

Rats displayed minimal discomfort and lacked overt signs of infection or chronic inflammation, with complete soft tissue and skin healing occurring normally regardless of the implant. Skulls were harvested at 1 week and 4 weeks postsurgery for evaluation of bone regeneration. Micro-computed tomography (uCT) analysis revealed complete coverage of the defect area (red circle) in both the autograft and BPLP-Ser/HA groups with their respective implants, highlighting the prolonged stability of BPLP-Ser/HA putty compared to resorbable Bone Waxes (Figure 7a). Isolation of the defect area revealed similar bone ingrowth around the periphery of all groups, indicating bone regeneration was successfully initiated (Figure 7b). After 4 weeks, BPLP-Ser/HA was no longer observed within the defect, confirming its degradable nature (the relatively rapid degradation of BPLP-Ser/HA in vivo compared to in vitro (4 weeks vs > 8 weeks) was likely mediated by active enzymatic degradation of polymers and active resorption of HA by

cells), while around 1/2 of the autograft had been resorbed (a common occurrence when large, living bone segments are separated from native vasculature and nutrient networks and a severe limitation in autografting procedures). Minimal bone growth was observed in the negative control and bone wax groups compared to week 1, while bone regeneration within the bone wax group even appeared lower than the negative control, in line with previous research demonstrating inhibited tissue regeneration in the presence of such nonresorbable materials.^[4] In contrast, significant bone ingrowth was seen in the autograft and BPLP-Ser/HA groups, with BPLP-Ser/HA appearing equivalent or superior. Quantitative bone volume to tissue volume (BV/TV) ratios were then extracted from uCT data (Figure 7c). No difference was observed among groups at 1 week; however, the BV/TV ratios of the autograft (21.01% ± 2.84%) and BPLP-Ser/HA (19.49% ± 2.79%) groups were higher than those of the negative control and bone wax at week 4, while no difference was observed between autograft and BPLP-Ser/HA. Indeed, BV/TV of both the negative control and bone wax groups barely increased from week 1 to week 4, in stark contrast to the more than four-fold increase in both the autograft and BPLP-Ser/HA groups. These results support the regenerative effects of BPLP-Ser/HA (equivalent to the gold standard autograft treatment) compared to conventional bone wax. Fluorescent imaging of tissue explants (Figure 7d) demonstrated strong green fluorescence of residual BPLP-Ser/HA at week 1, while at week 4

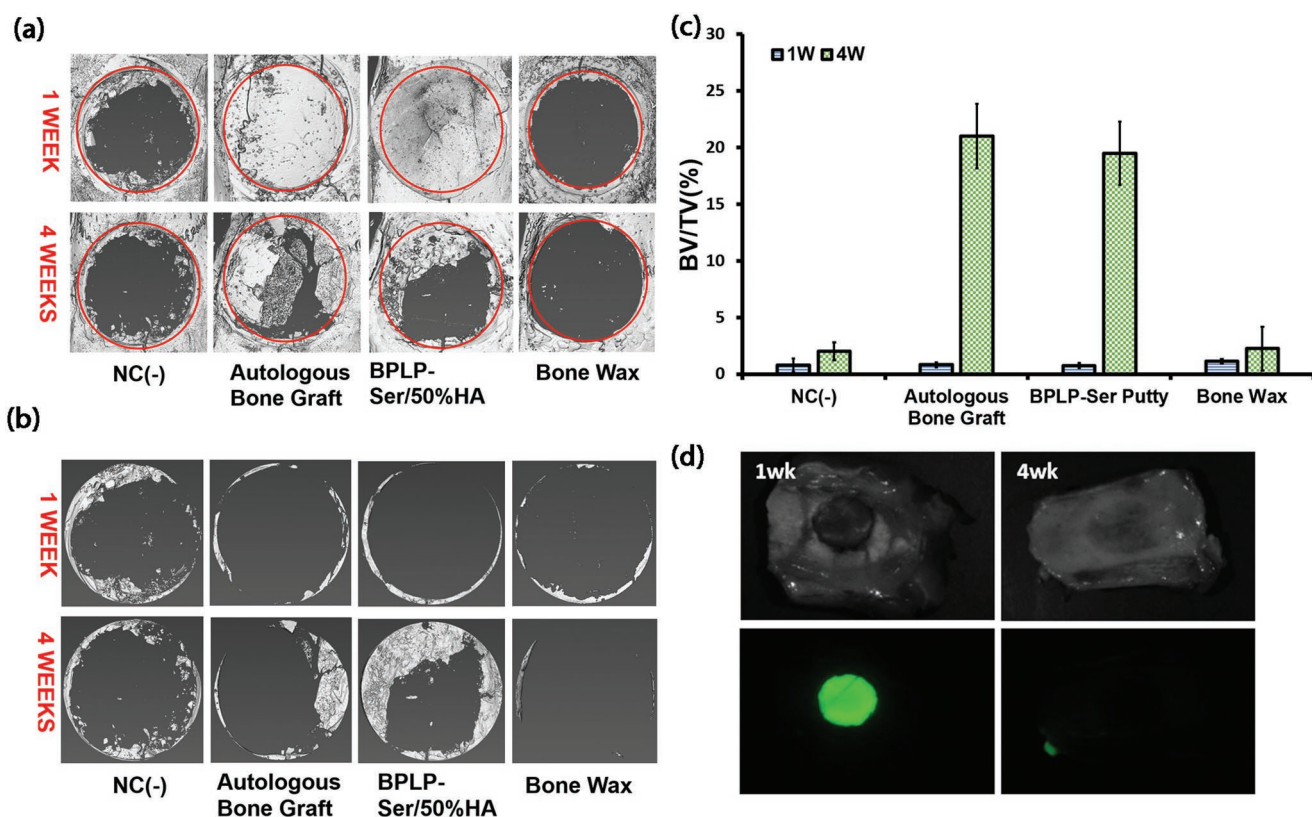


Figure 7. In vivo efficacy of BPLP-Ser/50%HA putty in critical-size cranial defects. a) Representative micro-computed tomography (uCT) scans 1 week and 4 weeks postsurgery (red circles indicate the original 8 mm defect diameter). b) uCT scans of regenerated cranial bone at 1 week and 4 weeks with remaining BPLP-Ser/50%HA and autograft removed to highlight new bone growth. c) Ratio of new bone volume to total volume at 1 week and 4 weeks. d) Remaining fluorescent signal of explanted materials at 1 and 4 weeks postsurgery. NC(-) = negative control. *n* = 3.

no fluorescent signal could be observed, confirming complete material degradation within 4 weeks while supporting the application of BPLP-SER/HA toward in vivo monitoring of material degradation.

Transverse defect sections were stained with hematoxylin and eosin (H&E) and compared to associated transverse uCT images to further examine tissue regeneration (Figure 8). Only loose fibrous tissue (indicative of early loose, nonmineralized mesenchyme tissue inherent in intramembranous ossification) was observed in the negative control and bone wax groups at

both week 1 and week 4 (Figure 8a,b,g,h) as confirmed by uCT. The presence of non-resorbable bone wax was also confirmed in the transverse uCT slices at week 1 and week 4. Autograft could be readily observed along with fibrous tissue at both 1 and 4 weeks (Figure 8c,d) while at week 4 resorption of the implant was evident along with new bone formation, consistent with the results from Figure 7. At week 1, fibrous tissue surrounded the BPLP-Ser/HA implant; however, it did not penetrate into the defect, while at week 4 significant new bone formation was observed in addition to fibrous tissue as well as

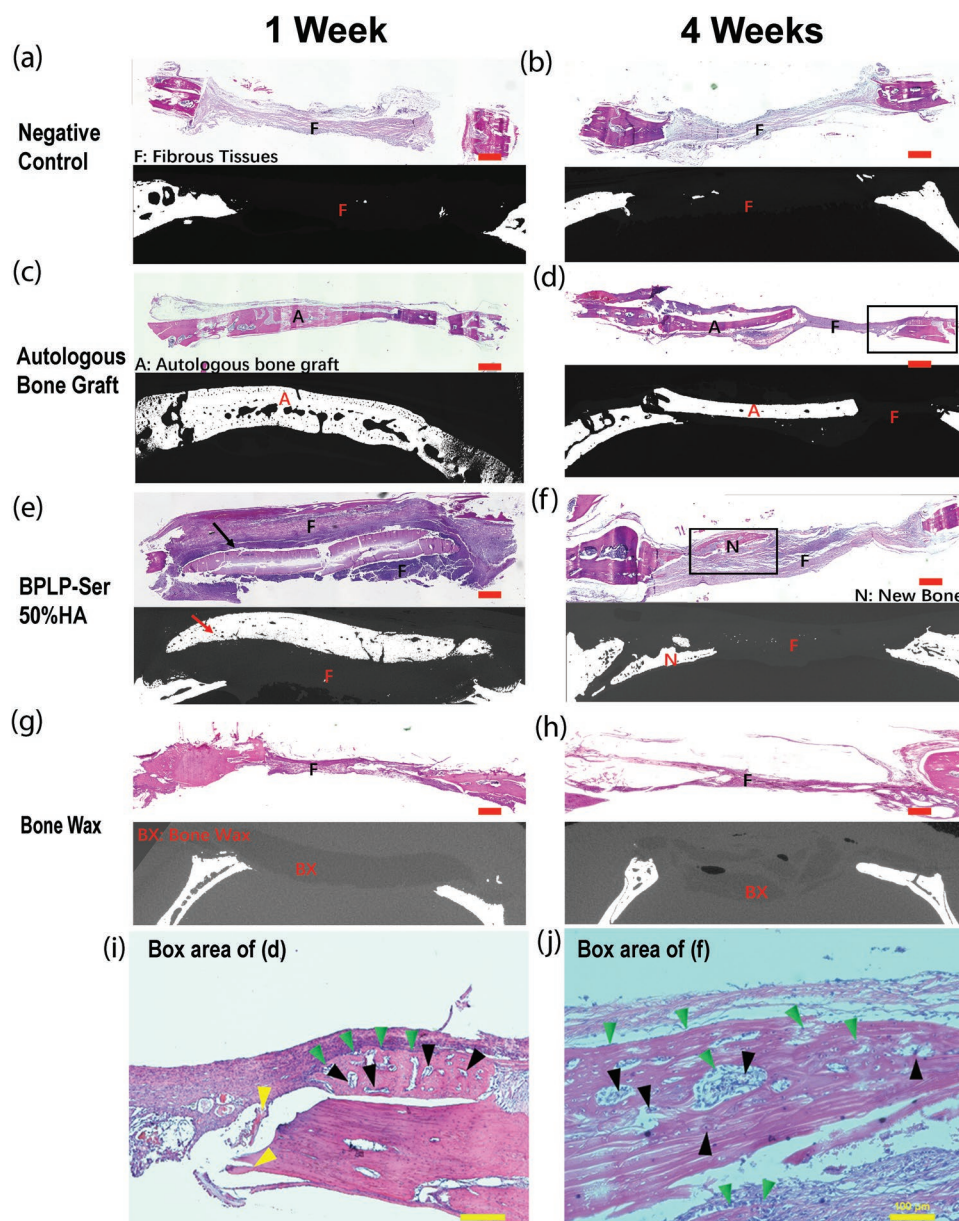


Figure 8. Histological results of cranial defect repair. Representative H&E-stained tissue sections and corresponding micro-computed tomography (μ CT) scans at 1 week and 4 weeks. a,b) negative control (NC(-)), c,d) autologous bone graft, e,f) BPLP-Ser/50%HA putty, and g,h) bone wax 1 week (a,c,e, and g) and 4 weeks (b,d,f, and h) postoperatively. Scale bar = 300 nm. Arrows indicate BPLP-Ser/50%HA putty. (i,j) Higher magnification images of the boxed region of (d) and (f), respectively. Scale bar = 100 μ m. “F” indicates fibrous repair tissue, “A” represents the autologous bone graft, “N” denotes new bone formation, and “BX” represents bone wax. In images (i and j), green triangles indicate osteoblasts, black triangles represent blood vessels, and yellow triangles mark residual autologous bone.

complete resorption of the implant (Figure 8e,f). The presence of macrophages was observed at week 1 in the bone wax, BPLP-Ser/HA, and negative groups, indicating an acute inflammatory response (Figure 8a,e,g); however, this was completely resolved in all groups by week 4, demonstrating that despite initial leaching of citrate from BPLP-Ser/HA materials, no significant chronic inflammation or adverse tissue response results. Additionally, at week 4, a denser fibrous tissue indicative of compact mesenchyme was observed in the BPLP-Ser and autograft groups compared to week 1 (Figure 8d,f), with large numbers of cells present, particularly adjacent to new bone (Figure 8i,j), further indicating regeneration of non-mineralized prebone tissue (indicating further development among the stages of intramembranous ossification: loose mesenchyme, compact mesenchyme, and formation of mineralized bone compared to the negative control and Bone Wax). At larger magnifications, osteoblasts were shown to be aligned along the surface of newly formed dense bone tissue in both the autograft and BPLP-Ser/HA groups (Figure 8i,j, respectively, green arrows), indicating active bone formation. Additionally, a large number of blood vessels were observed in both groups (black arrows), establishing critical neo-vasculature. Combined and supported by the uCT and BV/TV data, these findings confirm the regenerative potential of BPLP-Ser/HA as both superior to traditional bone wax and an equivalent alternative to autograft via the pro-osteogenic and angiogenic effects of citrate.

3. Conclusion

In summary, we have synthesized a new class of off-the-shelf, highly tunable citrate-based fluorescent putty-like materials as effective alternatives to clinically prevailing bone waxes. Leveraging the unique role of citrate as a bridge between the organic and inorganic phases of native bone, a strongly bound composite capable of homogeneously incorporating physiological levels of HA was obtained while maintaining soft mechanics and excellent handling. Obtained materials demonstrated hydration-induced strengthening in physiological conditions, tunable degradation rates, minimal swelling, promotion of blood clotting, hemostatic sealing potential, and enhanced adhesion to bone. Further, sustained citrate release enabled inherent antimicrobial and osteogenic potential. Finally, the novel reaction of L-Serine with citrate resulted in intrinsically fluorescent materials enabling ex vivo assessment of material degradation kinetics. Convergence of citrate's material-chemical and biological advantages in vivo led to calvaria bone regeneration greater than that obtained using commercial Bone Wax and equivalent to gold standard autograft. In the future, citrate-based putty is envisioned as a platform material benefitting from the significant tunability and modification potential of the citrate material family. For instance, degradation rates could be further extended via diol selection to accommodate differential tissue regeneration rates, enhanced bioactive properties could be incorporated via chemical conjugation or compositing, and fluorescence tracking could enable in vivo material monitoring. Citrate-based putty thus represents a new paradigm of intrinsically bioactive and multi-functional biomaterials toward effective clinical treatment of bone fractures and defects where the current bone wax is used.

4. Experimental Section

Materials: Hydroxyapatite (HA) (Mw: 502.32, assay > 90% (as Ca₅(PO₄)₃(OH))); particle size: > 75 μm (0.5%), 45–75 μm (1.4%), < 45 μm (98.1%) was purchased from Fluka (St. Louis, MO, USA). Commercial Bone Wax (ETH-W31G) was purchased from Ethicon (Cincinnati, OH, USA). Citrated bovine whole blood was purchased from Lampire Biological Laboratories (Pipersville, PA). All remaining chemicals were purchased from Sigma–Aldrich (St. Louis, MO, USA) and used as received unless stated otherwise.

Phase Purity Analysis of Hydroxyapatite: The phase purity of HA was assessed via X-ray diffraction (XRD) using an Empyrean II Diffractometer (Malvern Panalytical, Westborough, MA) from 0° to 80° 2θ and analyzed in JADE (MDI/ICCD, Newton Square, PA) (Figure S8, Supporting Information).

Biodegradable Photoluminescent Composite Putty Synthesis: Aliphatic biodegradable photoluminescent prepolymers were synthesized by the copolymerization of citric acid with 1,8-octanediol and L-serine in a 1.0:1.0:0.2 molar ratio. Briefly, a mixture of citric acid, 1,8-octanediol and L-serine were added to a 100 mL three-necked round bottom flask fitted with an inlet and outlet adapter. The mixture was melted under a flow of nitrogen gas by stirring at 160 °C in a silicone oil bath. The temperature of the system was subsequently lowered to 140 °C and allowed to react for 2 h to create a biodegradable photoluminescent prepolymer (pre-BPLP-Ser). To remove any of the unreacted monomers and oligomers, the prepolymer was dissolved in 1,4-dioxane and purified by drop wise precipitation in deionized water (DI) produced from a Direct-Q5 Water Purification System (Millipore, Billerica, MA). The undissolved prepolymer was collected and lyophilized in a Freezezone 6 Freeze Dryer (Labconco, Kansas City, MO) to obtain the purified preBPLP.

To synthesize fluorescent bone putties, pre-BPLP-Ser was composited with HA in various weight ratios. Briefly, pre-BPLP-Ser was dissolved in ethanol to create a 50 wt% solution. Next, HA was added to the solution at a predetermined wt% to pre-BPLP-Ser and mixed in a Teflon dish prewarmed to 80 °C to aid in solvent evaporation. The resulting putty was denoted as BPLP-Ser/X HA where X represents the HA weight percentage in the putty. For example, BPLP-Ser/50% HA indicates that 50 wt% HA was chosen for putty synthesis.

Composite Morphology: To assess the morphology and homogeneity of BPLP composites, disks 6 × 2 mm (diameter × height) were formed via press-fit into PDMS molds. Composites were subsequently removed, mounted for SEM imaging, and sputter coating with a 5 nm iridium layer (Emitec Sputter-Coater). Samples were imaged using an Apreo S LoVac SEM (Thermo Fisher Scientific, Waltham, MA). EDS analysis was conducted using AZtec (Oxford Instruments, Abingdon, UK).

Composite Mechanics: Unconfined compression tests were performed using a 5966 series advanced electromechanical testing system with a 10 kN load cell (Instron, Norwood, MA, USA). Briefly, cylindrical shaped samples 6.5 × 13 mm (diameter × height) were compressed at a rate of 1.3 mm min⁻¹ to 50% strain. Values were converted to stress-strain and the initial modulus (kPa) was calculated from the initial gradient of the resulting curve (0%–10% compressive strain). Wet mechanical properties were conducted as above on cylindrical samples incubated in phosphate-buffered saline (PBS) (pH 7.4), deionized (DI) water, or bovine whole blood at 37 °C under orbital shaking (200 rpm) for 24 h.

Composite Swelling: The swelling percentage was measured by the mass differential after incubation of the composite network in phosphate-buffered saline (PBS) at 37 °C under orbital shaking (200 rpm). Briefly, 6 × 2 mm (diameter × thickness) disc shaped samples were weighed to find the initial mass (W_i) and suspended in PBS for 24 h. The samples were removed from the PBS, blotted dry with filter paper, and weighed (W_s). The swelling percentage was calculated using the formula from Equation (1):

$$\text{Swelling(\%)} = (W_s - W_i) / W_i \times 100\% \quad (1)$$

Composite Degradation: The degradation rate of 6 × 2 mm (diameter × thickness) disk-shaped samples was assessed in vitro using phosphate-buffered saline (PBS) (pH 7.4) at 37 °C under orbital shaking (200 rpm). The PBS was changed every week to ensure that the pH did not drop below 7. Prior to weighing, samples were extensively rinsed with deionized water and lyophilized. Weight loss was calculated by

comparing the initial weight (W_i) with the weight measured at 1, 2, 4, 6, and 8 weeks (W_t), as shown in Equation (2).

$$\text{Mass loss(\%)} = (W_t - W_i) / W_i \times 100\% \quad (2)$$

pH of the degradation media was assessed at each time point using an Orion 4 Star Benchtop pH meter with an Orion 8102BN ROSS Combination pH Electrode (Thermo Fisher Scientific, Waltham, MA).

Composite Density: Composite Density was assessed using the density accessory for the Mettler Toledo XP504 balance (Mettler Toledo, Columbus, MN) at room temperature and with DI water as the auxiliary fluid. Briefly, 6×2 mm (diameter \times thickness) disk shaped samples were first weighed in the air to determine (W_a). Samples were then immersed in the auxiliary fluid bath to determine (W_b). Density was then calculated according to Equation (3):

$$\text{Density (g cm}^{-3}\text{)} = (W_a / (W_a - W_b)) \times (p_0 - p_L) + p_L \quad (3)$$

where p_0 = the density of DI water, and p_L = the density of air (0.0012 g cm^{-3}).

Photoluminescent Characterization: Photoluminescent properties of composites were studied using a Horiba FluoroMax-4 spectrofluorometer (Horiba Scientific, Edison, NJ). The fluorescent spectra of composites (1 cm diameter \times 2 mm thickness) were measured using a solid-state holder (Horiba Scientific, Edison NJ) with excitation and emission slit sizes of 1.5 nm by 1.5 nm and step size of 10 nm. Fluorescent images of composites were also obtained using an in vivo fluorescent imaging system (MaestroTM EX, Woburn, MA) with excitation and emission wavelengths of 370 and 580 nm, respectively.

Hemocompatibility: Hemocompatibility of bone wax and composites was assessed via a previously reported method.^[79,80,96] Briefly, 0.125 g of bone wax or BPLP-Ser composite was added to a 1.5 mL microcentrifuge tube and tamped with a Teflon rod to achieve uniform surface areas (500 μ L of PBS and 0.1% Triton X-100 solution in DI water served as negative and positive controls, respectively). Bovine whole blood was diluted 50x with PBS and 500 μ L of diluted blood was added to each sample followed by incubation at 37 °C with shaking (100 rpms) for 1 h. After 1 h, 500 μ L of PBS was added to bone wax and BPLP-Ser composite samples to normalize concentration with the positive and negative controls. Samples were then centrifuged at 2000 rpms for 10 min and 200 μ L of supernatant was pipetted into the wells of a 96 well plate. Absorbance was read at 545 nm using a plate reader (infinite M200 PRO, TECAN, Männedorf, Switzerland). Hemolysis (%) was calculated according to Equation (4):

$$\text{Hemolysis(\%)} = \left(\frac{A_s - A_{\text{neg}}}{A_{\text{pos}}} \right) \times 100 \quad (4)$$

where A_s = absorbance of the sample, A_{neg} = absorbance of the negative control, and A_{pos} = absorbance of the positive control.

Whole Blood Clotting Time: Blood clotting time of bone wax and composites was assessed according to a previously described method.^[79,80,96] 0.125 g of bone wax or BPLP-Ser composite was added to a 1.5 mL microcentrifuge tube and tamped with a Teflon rod to achieve uniform surface areas (blank microcentrifuge tubes served as a control). Citrated bovine whole blood was reactivated by mixing with 0.1M CaCl_2 (10% v/v) followed by mixing for 10 s. 100 μ L of blood was then added to each sample and samples were incubated at 37 °C. Clotting time was assessed via tilt testing every 30 s, with the formation of a nonflowable clot mass designated as the end point.

Hemostatic Sealing Test: Sealing capability of composites was assessed via a commonly utilized tube sealing method. Briefly, 2 mm vertical lengths of clear polyethylene tubing were attached to the wall of a 37 °C incubation room. Blue dye was then inserted via syringe attached to the top of the tube until the entire tube length was filled. Composite material was then inserted into the bottom of the tube to create a seal, after which the syringe was removed, exposing the composite to fluid pressure. The tube end was finally inserted into a beaker containing PBS.

Sealing time was then assessed with failure determined when dye was visible within the PBS contained within the beaker. Fluid pressure head in the tubes was determined via Equation (5):

$$\text{Pressure (mmHg)} = p \times g \times h \times 0.007501 \text{ mmHg N}^{-1} \quad (5)$$

where p = the density of DI water, g = gravitational force, and h = tube height, with a final pressure of 146.87 mmHg determined.

Adhesion Test: Adhesion strength to bone was assessed following a previous method with modifications.^[97] Deer bone was cut into rectangular sections ≈ 10 mm width \times 30 mm length \times 20 mm thickness to expose the trabeculae followed by rehydration in PBS for 1 h. Bone wax or BPLP-Ser composite (≈ 0.5 g) was then applied in a uniform layer to one 10 mm \times 30 mm bone face and a second bone face was then adhered to the first using hand pressure for 30 s. The attached bone pieces were then incubated in PBS for 24 h at 37 °C under agitation (200rpms). Adhesion strength was tested using a 5966 series advanced electromechanical testing system with a 10 kN load cell (Instron, Norwood, MA, USA) and 10 kN pneumatic tensile grips. One piece of the adhered bone was first placed within the top tensile grip followed by lowering the crosshead until the other piece was within the bottom grip, taking care not to grip the adhered interface. Tension was then applied at a rate of 1.3 mm min⁻¹ until failure of the adhesive, with peak stress calculated.

Adhesion to native tissue was also assessed qualitatively using chicken drumsticks. First, amputation was simulated via bisection of the femur, exposing the intramedullary cavity. The Composite was then packed into the cavity. Additionally, the femoral condyle was separated from the shaft, exposing the interior trabecular faces. BPLP composite was then gently pressed into the exposed face and used to reattach the separated condyle to the main body. Weight-bearing capability of the composite was then assessed by lifting the complete drumstick by the reattached condyle.

Cell Culture and Medium: Human mesenchymal stem cells (hMSCs, Lonza) were cultured in low glucose Dulbecco's Modified Eagle Medium (DMEM) with 10 vol.% fetal bovine serum (FBS) (Atlanta Biologicals, Flowery Branch, GA), GlutaMAX (Gibco Laboratories, Gaithersburg, MD), and 1% antibiotic antimycotic 100X solution (Invitrogen, Carlsbad, CA). L929 fibroblasts were cultured in DMEM with 10 vol. % FBS and 1% antibiotic antimycotic 100X solution and Eagle's Minimum Essential Medium (MEM) with 10 vol.% FBS 1% antibiotic antimycotic 100X solution.

Cytotoxicity: To prepare degradation products, 1 g of material was fully degraded in 10 mL 0.2 M NaOH solution followed by adjustment of pH to 7.4 with HCl and NaOH. Solutions were then centrifuged for 10 min at 12 000 rpms to fully remove undegraded HA. Degradation products were then sterilized via 0.2 μ m filter (Agilent, Santa Clara, CA). Dilutions of degradation products were prepared using a culture medium and 10 μ L of each dilution were added to L929 cells (with an initial cell density of 3600 per well) cultured in 96 well plates with 100 μ L medium. After culturing for 24 h, CCK-8 evaluation (Dojindo, Rockville, MD) was performed according to the manufacturer's instructions.

Cell Proliferation: For cell proliferation, degradation product dilutions were prepared using the above procedure. L929 cells with an initial density of 500 cells per well were cultured with chosen dilutions in 96-well plates (10 μ L per 100 μ L culture media as above). At designated time points, cell viability was examined by Cell Counting Kit-8 (Dojindo, Rockville, MD) according to manufacturer instructions. The proliferation of hMSCs seeded directly on the surface of BPLP-Ser/50%HA was also studied. hMSCs were seeded at an initial density of 3000 cells cm⁻². At designated time points (Day 1, 3, 7, and 14), cells were lysed with RIPA buffer, and DNA was quantified with the Pico Green dsDNA assay (Invitrogen, Carlsbad, CA) according to manufacturer instructions, with proliferation (%) on Days 3, 7, and 14 normalized to Day 1.

Cell Differentiation Study: hMSCs (<passage 6) were used to study differentiation in the presence of material degradation products. Briefly, cells at $\approx 80\%$ confluence were treated with an established OG medium (low-glucose DMEM with 10⁻⁷ M dexamethasone, 0.05 mM ascorbate-2-phosphate, and 0.01 M β -glycerophosphate) supplemented with

degradation products (prepared as above) at different concentrations for 14 days with pure OG medium as control.

ALP Assay: For ALP expression analysis, cell samples were lysed using RIPA buffer followed by centrifugation to remove debris. ALP activity was quantified utilizing p-nitrophenyl phosphate (PNPP) (hydrolyzed by ALP into a yellow-colored product). Briefly, PNPP stock solution (1M) was diluted with ALP assay buffer (1:100). 50 μ L of diluted buffer was then added to 50 μ L of lysate. After 10–30 min of incubation at 37 °C, absorbance was measured at 405 nm on a plate reader (infinite M200 PRO, TECAN, Männedorf, Switzerland).

Alizarin Red Staining: For Alizarin Red staining, cell samples were fixed with 4% paraformaldehyde. 40 mM Alizarin red solution was then added to fixed samples followed by 30 min of incubation with gentle shaking to stain calcium nodules. After thoroughly washing, the stained cells were observed via Microscope (Nikon, Tokyo, Japan).

Bacteria Incubation: *Staphylococcus aureus* (*S. aureus*, ATCC 6538) and *Escherichia coli* (*E. coli*, ATCC 25 922) were purchased from ATCC (American Type Culture Collection) and used following established safety protocols. Tryptic soy broth (Cat. #: C7141) and tryptic soy agar (Cat. #: C7121) used for *S. aureus* culture were purchased from Criterion (through VWR). Luria broth base (LB broth, Cat. #: 12795-027) and select agar (Cat. #: 30391-023) used for *E. coli* culture were purchased from Invitrogen. *S. aureus* and *E. coli* were incubated at 37 °C in sterilized tryptic soy broth and LB broth, respectively, with a speed of 150 rpm in a rotary shaker overnight and the obtained bacteria suspensions were diluted to a 0.5 McFarland Standard (optical density (OD) at 600 nm around 0.06 and 0.034 for *S. aureus* and *E. coli*, respectively).

Bacterial Inhibition: The bacterial inhibition of BPLP-Ser/HA putty against both *S. aureus* and *E. coli* was tested via turbidity assay. For each sample, 20 mg of ethylene oxide sterilized material was placed in a 96 well plate and immersed in 200 μ L of germ containing nutrient solution with a bacterial concentration of 1×10^6 (CFU) per mL (100x dilution from 0.5 McFarland Standard). Incubation was performed at 37 °C on an orbital shaker with a speed of 150 rpm for 24 h. Germ containing growth broth, pure growth broth without bacteria, and commercial bone wax were also tested and served as positive, negative, and material controls, respectively. The bacterial broth medium was then aliquoted, and the OD value of the medium at 600 nm was recorded by a microreader (TECAN, infinite M200 PRO). The inhibition ratios were calculated by Equation (6):

$$\text{Inhibition Ratio(\%)} = 100 - 100 \times \frac{A_t - A_0}{A_{con} - A_0} \quad (6)$$

where A_0 is the OD value of bacterial broth medium before incubation, and A_t and A_{con} are the OD values of material containing medium and germ containing growth medium (control) after incubation, respectively

Rat Critical-Sized Cranial Model: The rat experiments were performed in compliance with a protocol approved by the Institutional Animal Care and Use Committee (IACUC, Approval Number: PRAMS201342878) at the Pennsylvania State University. Sprague-Dawley rats (male, age 8–12 weeks, \approx 200 g) were randomly divided into four groups of 6 rats per group for in vivo evaluation of BPLP composites. Rats were anesthetized by inhalation of 2%–4% isoflurane gas until unresponsive followed by a supplement of ketamine and xylazine anesthesia (80 mg kg^{-1} and 10 mg kg^{-1} , respectively). Local anesthesia, buprenorphine, and bupivacaine were then injected subcutaneously at the parietal site. The surgical site was shaved and disinfected by swabbing with 10% povidone iodine solution followed by 70% alcohol and sterile saline swabs. The calvarium was exposed after skin incision (Figure S6a, Supporting Information) followed by trephining a circular 8 mm diameter cranial bone defect using a low-speed dental drill (Foredom, Bethel, CT) (1500 rpm) with saline irrigation to prevent friction-based thermal damage to surrounding tissues (Figure S6b,c, Supporting Information). The cranial disk was removed and care was taken not to damage the underlying dura mater (Figure S6d,e, Supporting Information). The site was then flushed with sterile saline solution and the defects were filled with either 0.25 g

of BPLP-Ser/50%HA composite or bone wax without applying pressure on the underlying brain (Figures S6f and S7, Supporting Information). Autogenous cranial bone was rotated 180° and replaced within the defect to serve as positive control, while defects sans material served as the negative control. The periosteum and skin tissue were closed and sutured with 6–0 VICRYL absorbable sutures. Rats were euthanized 1 week and 4 weeks postsurgery via carbon dioxide. At each time point, the heads were separated post euthanasia followed by dissection and isolation of the cranial defect for subsequent micro-CT scanning and histology. All animal experiments were carried out in compliance with protocols approved by the Pennsylvania State University Institutional Animal Care and Use Committee.

μ CT Analysis: Micro CT imaging was performed using a General Electric ν tome|x L300 nano/microCT (General Electric, Boston, MA) dual-tube system equipped with a 300 kV unipolar microfocus X-ray tube, a 180 kV nanofocus X-ray tube with transmission target assembly, and a GE DXR250 high-contrast digital flat panel detector. Volumes of interest were selected in Avizo (FEI Company, Hillsboro, OR) from which % bone volume/total volume (BV/TV) was calculated. VOI was defined using an 8 mm cylinder (the original defect diameter) with a height greater than the thickness of the defect (\approx 2 mm). Thresholding values of new bone were chosen to match the average density value of the native bone by sampling the latter in the region adjacent to but outside the 8 mm circular region of interest (ROI) corresponding to the surgically created defect. Threshold values for the BPLP-Ser/50%HA were likewise chosen via an average of the density of the material measured within its bulk.

Histology: Calvarial bones were fixed in 4% cold paraformaldehyde for 24 h at 4 °C. Remaining BPLP-Ser/50%HA in the explants was imaged using an in vivo fluorescent imaging system (MaestroTM EX, Woburn, MA) with excitation and emission wavelengths of 370 and 580 nm, respectively. The bone was then decalcified in 12.5% EDTA and 12.5% 4% paraformaldehyde in 1x phosphate-buffered saline (PBS) (pH 7.4) for 8 weeks. Fully decalcified bones were dehydrated in an ascending ethanol series and infiltrated with paraffin wax by a TP1020 tissue processor (Leica, Buffalo Grove, IL). Samples were embedded in wax and 8 μ m serial slices were sectioned via microtome (Shandon, Charleston, SC). Slices were placed on positively charged microscope slides and dried overnight. The sections were then stained with H&E using an Autostainer XL (Leica, Buffalo Grove, IL) and observed under light microscopy (Keyence, Woburn, MA).

Statistical Methods: All data was recorded as mean \pm standard deviation (SD), unless otherwise stated. Data was analyzed using Microsoft Excel software. For all studies, statistical analysis was performed via one way analysis of variance (ANOVA). Statistical significance was indicated by * $p < 0.05$, and sample number n was specifically stated.

Supporting Information

Supporting Information is available from the Wiley Online Library or from the author.

Acknowledgements

X.T., E.G., and Y.W. contributed equally to this work. This work was supported in part by a National Institute of Arthritis and Musculoskeletal and Skin Diseases (NIAMS) award (AR072731).

Conflict of Interest

Dr. Jian Yang and The Pennsylvania State University have a financial interest in Acuitive Technologies, Inc. and Aleo BME, Inc. These interests have been reviewed by the University's Institutional and Individual Conflict of Interest Committees and are currently being managed by the University.

Data Availability Statement

Research data are not shared.

Keywords

bone putty, bone wax, citric acid, metabonegenesis, orthopedic biomaterials

Received: May 15, 2022

Published online:

- [1] M. Massimo, R. A. Timothy, *Bone Res.* **2013**, *1*, 203.
- [2] N. Allen-Wilson, R. Beatty, J. Sharpe, *J. Am. Podiatr. Med. Assoc.* **2015**, *105*, 74.
- [3] S. Claudio, T. Enrico, B. Giuseppe, A. Vincenzo, M. Aldo, *Eur. Spine J.* **2004**, *13*, S89.
- [4] Z. Huan, G. Jun, B. Yanjie, L. Chunyong, Y. Lei, *J. Orthop. Transl.* **2019**, *17*, 64.
- [5] G. Laurel, K. Anthony, W. Philip, E. C. John Jr., *Infect. Control Hosp. Epidemiol.* **2004**, *25*, 346.
- [6] A. Fahradyan, L. Ohanisian, M. Tsuha, M. J. Park, J. A. Hammoudeh, *J. Craniofacial Surg.* **2018**, *29*, 976.
- [7] W. Tadeusz, H. A. Yuehuei, W. Xuejun, K. Qian, M. H. Christopher, K. A. Jonathan, *Clin. Orthop. Relat. Res.* **2008**, *466*, 481.
- [8] J. Suwanprateeb, W. Suvannapruk, F. Thammarakcharoen, W. Chokevivat, P. Rukskul, *J. Mater. Sci.: Mater. Med.* **2013**, *24*, 2881.
- [9] A. Ihsanul, S. Heroe, Puruhito, *Asian Cardiovasc. Thorac. Ann.* **2020**, *29*, 203.
- [10] D. P. Orgill, F. W. Ehret, J. F. Regan, J. Glowacki, J. B. Mulliken, *J. Biomed. Mater. Res.* **39**, 358.
- [11] W. Wassanai, Q. Timothy, P. Suthipas, *Solid State Phenom.* **2017**, *266*, 221.
- [12] C. Weijing, Z. Shouyang, Z. Yin, Q. Fan, T. Jun, W. Zhenning, L. Jiapan, *Mater. Sci. Eng., C* **2019**, *99*, 979.
- [13] L. Jiaying, H. Yang, L. Long, W. Chao, W. Jia, L. Yang, C. Dafu, D. Xiaokang, S. Chuanan, X. Fujian, *Adv. Sci.* **2020**, *7*, 2002243.
- [14] Y. Feifei, L. Minchao, Z. Tie, Z. Qi, C. Yan, L. Zhibo, W. Renxiong, C. Lin, *ACS Biomater. Sci. Eng.* **2021**, *7*, 663.
- [15] K. Saeid, B. Francesco, H. Sepideh, G. H. Robert, M. Masoud, *Trends Biotechnol.* **2018**, *36*, 430.
- [16] D. Xie, J. Guo, M. Mehdizadeh, R. T. Tran, R. Chen, D. Sun, G. Qian, D. Jin, X. Bai, J. Yang, *J. Mater. Chem. B* **2015**, *3*, 387.
- [17] S. Bai, X. Zhang, X. Lv, M. Zhang, X. Huang, Y. Shi, C. Lu, J. Song, H. Yang, *Adv. Funct. Mater.* **2020**, *30*, 1908381.
- [18] S. Tarafder, G. Y. Park, J. Felix, C. H. Lee, *Acta Biomater.* **2020**, *117*, 77.
- [19] J. Yang, A. R. Webb, G. A. Ameer, *Adv. Mater.* **2004**, *16*, 511.
- [20] D. Motlagh, J. Allen, R. Hoshi, J. Yang, K. Lui, G. Ameer, *J. Biomed. Mater. Res., Part A* **2007**, *82*, 907.
- [21] L.-C. Su, Z. Xie, Y. Zhang, K. T. Nguyen, J. Yang, *Front. Bioeng. Biotechnol.* **2014**, *2*, 23.
- [22] J. Guo, Z. Xie, R. T. Tran, D. Xie, D. Jin, X. Bai, J. Yang, *Adv. Mater.* **2014**, *26*, 1906.
- [23] J. Dey, H. Xu, K. T. Nguyen, J. Yang, *J. Biomed. Mater. Res., Part A* **2010**, *95*, 361.
- [24] D. W. Sun, Y. H. Chen, R. T. Tran, S. Xu, D. H. Xie, C. H. Jia, Y. C. Wang, Y. Guo, Z. M. Zhang, J. S. Guo, J. Yang, D. Jin, X. C. Bai, *Sci. Rep.* **2014**, *4*, 1.
- [25] J. S. Guo, Z. W. Xie, R. T. Tran, D. H. Xie, D. D. Jin, X. C. Bai, J. Yang, *Adv. Mater.* **2014**, *26*, 1906.
- [26] J. Dey, R. T. Tran, J. Shen, L. Tang, J. Yang, *Macromol. Mater. Eng.* **2011**, *296*, 1149.
- [27] D. Gyawali, P. Nair, Y. Zhang, R. T. Tran, C. Zhang, M. Samchukov, M. Makarov, H. K. W. Kim, J. A. Yang, *Biomaterials* **2010**, *31*, 9092.
- [28] R. T. Tran, P. Thevenot, D. Gyawali, J. C. Chiao, L. Tang, J. Yang, *Soft Matter* **2010**, *6*, 2449.
- [29] Y. Jiao, D. Gyawali, J. M. Stark, P. Akcora, P. Nair, R. T. Tran, J. Yang, *Soft Matter* **2012**, *8*, 1499.
- [30] R. T. Tran, M. Palmer, S. J. Tang, T. L. Abell, J. Yang, *Gastrointest. Endosc.* **2012**, *75*, 1092.
- [31] J. Yang, Y. Zhang, S. Gautam, L. Liu, J. Dey, W. Chen, R. P. Mason, C. A. Serrano, K. A. Schug, L. Tang, *Proc. Natl. Acad. Sci. USA* **2009**, *106*, 10086.
- [32] Z. W. Xie, Y. Zhang, L. Liu, H. Weng, R. P. Mason, L. P. Tang, K. T. Nguyen, J. T. Hsieh, J. Yang, *Adv. Mater.* **2014**, *26*, 4491.
- [33] Y. Zhang, R. T. Tran, I. S. Qattan, Y. T. Tsai, L. P. Tang, C. Liu, J. Yang, *Biomaterials* **2013**, *34*, 4048.
- [34] J. Q. Hu, J. S. Guo, Z. W. Xie, D. Y. Shan, E. Gerhard, G. Y. Qian, J. Yang, *Acta Biomater.* **2016**, *29*, 307.
- [35] M. Mehdizadeh, H. Weng, D. Gyawali, L. Tang, J. Yang, *Biomaterials* **2012**, *33*, 7972.
- [36] J. Guo, G. B. Kim, D. Shan, J. P. Kim, J. Hu, W. Wang, F. G. Hamad, G. Qian, E. B. Rizk, J. Yang, *Biomaterials* **2017**, *112*, 275.
- [37] L. C. Su, Z. Xie, Y. Zhang, K. T. Nguyen, J. Yang, *Front. Bioeng. Biotechnol.* **2014**, *2*, 23.
- [38] Q. Hongjin, Y. Jian, K. Pradeep, K. Jason, A. A. Guillermo, *Biomaterials* **2006**, *27*, 5845.
- [39] Y. Jian, Z. Yi, G. Santosh, L. Li, D. Jagannath, C. Wei, P. M. Ralph, A. S. Carlos, A. S. Kevin, T. Liping, *Proc. Natl. Acad. Sci. USA* **2009**, *106*, 10086.
- [40] J. P. Kim, Z. W. Xie, M. Creer, Z. W. Liu, J. Yang, *Chem. Sci.* **2017**, *8*, 550.
- [41] C. Ma, X. Tian, J. P. Kim, D. Xie, X. Ao, D. Shan, Q. Lin, M. R. Hudock, X. Bai, J. Yang, *Proc. Natl. Acad. Sci. USA* **2018**, *115*, E11741.
- [42] C. Y. Ma, M. L. Kuzma, X. O. C. Bai, J. Yang, *Adv. Sci.* **2019**, *6*, e1900819.
- [43] E. Al-Sharifi, N. Alkaisy, A. Al-Mahmood, *Biomed. Res.* **2019**, *30*, 406.
- [44] Y. Cui, T. Zhu, A. Li, B. Liu, Z. Cui, Y. Qiao, Y. Tian, D. Qiu, *ACS Appl. Mater. Interfaces* **2018**, *10*, 6956.
- [45] X. Zheng, Y. Liu, Y. Liu, Y. Pan, Q. Yao, *J. Biomed. Mater. Res., Part B* **2021**, *109*, 517.
- [46] S. P. Soundarya, A. H. Menon, S. V. Chandran, N. Selvamurugan, *Int. J. Biol. Macromol.* **2018**, *119*, 1228.
- [47] D. Zhang, X. Wu, J. Chen, K. Lin, *Bioact. Mater.* **2018**, *3*, 129.
- [48] M. Alizadeh-Osgouei, Y. Li, C. Wen, *Bioact. Mater.* **2019**, *4*, 22.
- [49] G. L. Koons, M. Diba, A. G. Mikos, *Nat. Rev. Mater.* **2020**, *5*, 584.
- [50] J. Tang, J. Guo, Z. Li, C. Yang, D. Xie, J. Chen, S. Li, S. Li, G. B. Kim, X. Bai, *J. Mater. Chem. B* **2015**, *3*, 5569.
- [51] D. Xie, J. Guo, M. R. Mehdizadeh, R. T. Tran, R. Chen, D. Sun, G. Qian, D. Jin, X. Bai, J. Yang, *J. Mater. Chem. B* **2015**, *3*, 387.
- [52] J. Guo, X. Tian, D. Xie, K. Rahn, E. Gerhard, M. L. Kuzma, D. Zhou, C. Dong, X. Bai, Z. Lu, *Adv. Funct. Mater.* **2020**, *30*, 2002438.
- [53] X. Qiu, L. Chen, J. Hu, J. Sun, Z. Hong, A. Liu, X. Chen, X. Jing, *J. Polym. Sci., Part A: Polym. Chem.* **2005**, *43*, 5177.
- [54] R. Xie, J. Hu, F. Ng, L. Tan, T. Qin, M. Zhang, X. Guo, *Ceram. Int.* **2017**, *43*, 4794.
- [55] Z. Wang, L. Chen, Y. Wang, X. Chen, P. Zhang, *ACS Appl. Mater. Interfaces* **2016**, *8*, 26559.
- [56] H. Nabipour, S. Batool, Y. Hu, *Emergent Mater.* **2021**, *1*.
- [57] W. Jiang, G. Griffanti, F. Tamimi, M. D. McKee, S. N. Nazhat, *J. Struct. Biol.* **2020**, *212*, 107592.
- [58] C. Shao, R. Zhao, S. Jiang, S. Yao, Z. Wu, B. Jin, Y. Yang, H. Pan, R. Tang, *Adv. Mater.* **2018**, *30*, 1.
- [59] E. Ruiz-Agudo, C. Ruiz-Agudo, F. Di Lorenzo, P. Alvarez-Lloret, A. Ibañez-Velasco, C. Rodríguez-Navarro, *ACS Biomater. Sci. Eng.* **2021**, *2346*.

- [60] E. Davies, K. H. Müller, W. C. Wong, C. J. Pickard, D. G. Reid, J. N. Skepper, M. J. Duer, *Proc. Natl. Acad. Sci. USA* **2014**, *111*, E1354.
- [61] Y.-Y. Hu, A. Rawal, K. Schmidt-Rohr, *Proc. Natl. Acad. Sci. USA* **2010**, *107*, 22425.
- [62] J. Zeng, S. Yang, H. Yu, Z. Xu, X. Quan, J. Zhou, *Langmuir* **2021**, *37*, 3410.
- [63] Z. Xie, J. P. Kim, Q. Cai, Y. Zhang, J. Guo, R. S. Dhimi, L. Li, B. Kong, Y. Su, K. A. Schug, J. Yang, *Acta Biomater.* **2017**, *50*, 361.
- [64] R. T. Tran, L. Wang, C. Zhang, M. Huang, W. Tang, C. Zhang, Z. Zhang, D. Jin, B. Banik, J. L. Brown, *J. Biomed. Mater. Res., Part A* **2014**, *102*, 2521.
- [65] D. B. Burr, M. R. Allen, *Basic and Applied Bone Biology*, Academic Press, Burlington, MA **2019**.
- [66] B. M. Willie, A. Petersen, K. Schmidt-Bleek, A. Cipitria, M. Mehta, P. Strube, J. Lienau, B. Wildemann, P. Fratzl, G. Duda, *Soft Matter* **2010**, *6*, 4976.
- [67] B. Zhang, J. E. DeBartolo, J. Song, *ACS Appl. Mater. Interfaces* **2017**, *9*, 4450.
- [68] M. C. Serrano, L. Carbajal, G. A. Ameer, *Adv. Mater.* **2011**, *23*, 2211.
- [69] S. Zaky, K. Lee, J. Gao, A. Jensen, K. Verdelis, Y. Wang, A. Almarza, C. Sfeir, *Acta Biomater.* **2017**, *54*, 95.
- [70] H. Lv, H. Wang, Z. Zhang, W. Yang, W. Liu, Y. Li, L. Li, *Life Sci.* **2017**, *178*, 42.
- [71] D. Shan, S. R. Kothapalli, D. J. Ravnic, E. Gerhard, J. P. Kim, J. Guo, C. Ma, J. Guo, L. Gui, L. Sun, *Adv. Funct. Mater.* **2018**, *28*, 1801787.
- [72] J. Pfeilschifter, G. R. Mundy, *Proc. Natl. Acad. Sci. USA* **1987**, *84*, 2024.
- [73] X. Lu, S. Shi, H. Li, E. Gerhard, Z. Lu, X. Tan, W. Li, K. M. Rahn, D. Xie, G. Xu, *Biomaterials* **2020**, *232*, 119719.
- [74] J. Peterson, P. C. Dechow, *The Anatomical Record Part A: Discoveries in Molecular, Cellular, and Evolutionary Biology*, Wiley-VCH, **2003**, pp. 785–797.
- [75] N. Nooh, W. A. Abdullah, M. E.-A. Grawish, S. Ramalingam, F. Javed, K. Al-Hezaimi, *Indian J. Orthop.* **2014**, *48*, 319.
- [76] J. Suwanprateeb, W. Suvannapruk, F. Thammarakcharoen, W. Chokevivat, P. Rukskul, *J. Mater. Sci.: Mater. Med.* **2013**, *24*, 2881.
- [77] O. Y. Golubeva, N. Y. Ulyanova, E. V. Vladimirova, O. V. Shamova, *Langmuir* **2021**, *37*, 12356.
- [78] I. Ivanov, *Biochim. Biophys. Acta, Biomembr.* **1999**, *1415*, 349.
- [79] R. K. Avery, H. Albadawi, M. Akbari, Y. S. Zhang, M. J. Duggan, D. V. Sahani, B. D. Olsen, A. Khademhosseini, R. Oklu, *Sci. Transl. Med.* **2016**, *8*, 365ra156.
- [80] A. K. Gaharwar, R. K. Avery, A. Assmann, A. Paul, G. H. McKinley, A. Khademhosseini, B. D. Olsen, *ACS Nano* **2014**, *8*, 9833.
- [81] V. A. Kumar, N. L. Taylor, A. A. Jalan, L. K. Hwang, B. K. Wang, J. D. Hartgerink, *Biomacromolecules* **2014**, *15*, 1484.
- [82] T. Brückner, M. Schamel, A. C. Kübler, J. Groll, U. Gbureck, *Acta Biomater.* **2016**, *33*, 252.
- [83] R. Macfarlane, *J. Clin. Pathol.* **1948**, *1*, 113.
- [84] A. H. Hofman, I. A. van Hees, J. Yang, M. Kamperman, *Adv. Mater.* **2018**, *30*, 1704640.
- [85] Y. Xiong, X. Zhang, X. Ma, W. Wang, F. Yan, X. Zhao, X. Chu, W. Xu, C. Sun, *Polym. Chem.* **2021**, 3721.
- [86] S. Duan, R. Wu, Y.-H. Xiong, H.-M. Ren, C. Lei, Y.-Q. Zhao, X.-Y. Zhang, F.-J. Xu, *Prog. Mater. Sci.* **2021**, *125*, 100887.
- [87] S. Mittapally, R. Taranum, S. Parveen, *J. Drug Delivery Ther.* **2018**, *8*, 411.
- [88] J. Guo, W. Wang, J. Hu, D. Xie, E. Gerhard, M. Nisic, D. Shan, G. Qian, S. Zheng, J. Yang, *Biomaterials* **2016**, *85*, 204.
- [89] C. Ma, E. Gerhard, D. Lu, J. Yang, *Biomaterials* **2018**, *178*, 383.
- [90] C. Ma, E. Gerhard, Q. Lin, S. Xia, A. D. Armstrong, J. Yang, *Bioact. Mater.* **2018**, *3*, 19.
- [91] G. Thalji, C. Gretzer, L. F. Cooper, *Bone* **2013**, *52*, 444.
- [92] D. Granchi, E. Torreggiani, A. Massa, R. Caudarella, G. Di Pompo, N. Baldini, *PLoS One* **2017**, *12*, e0181230.
- [93] Y. He, Q. Y. Li, C. Y. Ma, D. H. Xie, L. M. Li, Y. T. Zhao, D. Y. Shan, S. K. Chomos, C. Dong, J. W. Tierney, L. Sun, D. Lu, L. Gui, J. Yang, *Acta Biomater.* **2019**, *93*, 180.
- [94] L. Dupoirieux, D. Pourquier, M. Picot, M. Neves, *Int. J. Oral Maxillofac. Surg.* **2001**, *30*, 58.
- [95] P. P. Spicer, J. D. Kretlow, S. Young, J. A. Jansen, F. K. Kasper, A. G. Mikos, *Nat. Protoc.* **2012**, *7*, 1918.
- [96] H. Albadawi, I. Altun, J. Hu, Z. Zhang, A. Panda, H. J. Kim, A. Khademhosseini, R. Oklu, *Adv. Sci.* **2021**, *8*, 2003327.
- [97] A. Bou-Francis, A. Ghanem, *Int. J. Adhes. Adhes.* **2017**, *77*, 96.